Electroexcitation of nuclear magnetic dipole transitions

Lawrence W. Fagg*†

Naval Research Laboratory, Washington, D.C. 20375

The field of electroexcitation of nuclear M1 transitions is reviewed. The subject is introduced with an elementary description of the relationship between backward-angle electron scattering and M1 excitation. Data analysis methods as well as 180° electron scattering techniques are also treated. The discussion of experimental results emphasizes the strength of the spin–flip transition, the concentration of M1 strength in self-conjugate nuclei, the degree of fragmentation of this strength in other nuclei, the response of odd-A rotational nuclei to 180° electron scattering, and the possible existence of an M1 giant resonance among the nuclides, especially the heavy nuclei.

CONTENTS

I. Introduction 683
II. Theoretical Survey 684
A. Relationship between backward angle scattering and M1 transitions 684
B. Nuclear properties studied at backward angles 685
1. Plane wave Born approximation 685
2. Distorted wave Born approximation 687
C. Radiation tails and radiative corrections 689
III. Remarks on Experimental Techniques Peculiar to 180° Scattering 691
IV. Discussion of Experimental Results 694
A. Self-conjugate nuclei 694
1. Theoretical preliminaries–sum rules 694
2. The deuteron 696
3. p- and sd-shell nuclei 697
B. Non-self-conjugate nuclei 700
1. Preliminary remarks 700
2. $A < 40$ Nuclei 700
3. $A > 40$ Nuclei 702
V. Table of Results and Glossary of Symbols 704
VI. Conclusions and Suggestions for Further Study 708
VII. Acknowledgments 708

I. INTRODUCTION

Magnetic dipole (M1) transitions enjoy a relatively unique position in the study of nuclear structure properties. Since the M1 operator is mostly an isovector and mostly a spin operator (Yoshida and Zamick, 1972), M1 transitions are especially suitable for probing the spin and isospin characteristics of the nucleus. This ability is dramatically exhibited in the many especially strong spin-flip transitions throughout the nuclides and in the spin- and isospin-flip transitions in the self-conjugate nuclei. Thus M1 transitions can test basic selection rules, help determine the role of the spin-flip mechanism in transitions, and furnish valuable knowledge of isospin mixing and splitting effects. Indeed knowledge of the distribution of M1 strength in a nucleus can give information on the spin dependence of the nuclear force (Hanna, 1974).

In many nuclei the sum strength of observed M1 transitions exhausts a major portion of the applicable sum rules (Hanna, 1974). Generally such sums are directly related to the ground-state spin-orbit coupling expectation value and thus serve as a test for intermediate coupling schemes and ground state deformations. Since Siegert's theorem (Siegert, 1937) interdicts the presence of meson exchange currents in E1 transitions, M1 transitions offer a means of detecting such exchange effects, especially in the deuteron and other light nuclei where other effects, such as configuration mixing are not a problem. Finally, evidence has been growing, primarily as the result of interest in recent years, for the existence of a giant M1 resonance throughout the nuclides comparable in universality to the well-known E1 resonance.

Perhaps the most powerful means of observing ground-state M1 transitions, and indeed magnetic multipole transitions generally, is afforded by the selective excitation of such transitions by backward angle electron scattering, particularly 180° electron scattering. This very selectivity has served to delimit a subfield of nuclear physics that can properly be called "Electroexcitation of Magnetic Dipole Transitions." Barber and his collaborators (Barber *et al.*, 1960; Barber, 1962) essentially founded this field with their early survey results using backward angle electron scattering.

Two articles that have to some extent reviewed the field were written by Barber (1962) and by Goldemberg and Pratt (1966) roughly a decade ago. The former article was actually a review of inelastic electron scattering in general at an early stage of its development and included discussions of pertinent scattering theory, experimental techniques, and the then current experimental results. The latter paper, although dealing essentially with magnetic electron scattering, elastic and inelastic, was primarily devoted to theory and to the extraction and interpretation of information on nuclear structure in general, with little discussion of results of work on specific nuclei.

More recently Theissen (1972), reviewing the inelastic electron scattering from light nuclei, has discussed the associated experimental apparatus, data analysis, and experimental results. Whereas the Theissen article has indeed dealt with some more recently electroexcited M1 transitions, its coverage is limited to the light nuclei and the primary thrust of the article is not directed to magnetic inelastic scattering.

* This paper is a considerably expanded version of an earlier outline on this subject (Fagg, 1973).

† This work was done in part under the auspices of the Aspen Center for Physics, Aspen, Colorado.

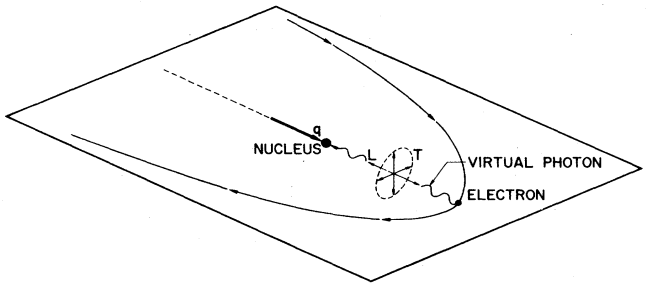

FIG. 1. Definition of longitudinal and transverse virtual photon polarizations with respect to momentum transfer direction [figure from Fagg (1973)].

Under these circumstances it was felt that a review of the electroexcitation of M1 transitions in nuclei at this time would be useful. Furthermore, such a review would be quite timely since a summary of the first major phases of the effort in this area could serve as a basis for the more precise work expected with the new round of higher resolution, higher current Linac facilities (e.g., Bates-M.I.T., Darmstadt, Amsterdam, Saclay) presently emerging. Thus this article will present relevant theoretical considerations, and discuss and summarize the known electroexcited M1 transitions in nuclei at low momentum transfers (<100 MeV/c). No claim of ultimate completeness in coverage is made.[1] The presentation throughout will be made from as elementary and conceptual a point of view as feasible.

Accordingly, Sec. II presents a theoretical survey in which considerable emphasis is placed on an examination of the intimate relationship between backward angle electron scattering and excitation of M1 transitions. The nuclear properties that can be studied in backward angle scattering along with Coulomb distortion effects are then discussed. Also some remarks on radiative tails and corrections relevant to backward scattering are included. Section III mentions some of the more significant 180° scattering techniques and associated experimental methods. The main body of the experimental results are discussed in Sec. IV. Because of their uniqueness, the self-conjugate nuclei are the subject of a separate subsection prefaced with some appropriate theoretical remarks, again of a most elementary nature. A summary table of experimental results and a glossary of symbols used throughout the paper are presented in Sec. V. Section VI consists of some concluding remarks along with suggestions for further study.

II. THEORETICAL SURVEY

A. Relationship between backward angle scattering and M1 transitions

The intimate relationship between backward angle scattering and excitation of M1 transitions, being the foundation on which the field treated in this paper is based, will be examined using an elemental and descriptive approach. In order to simplify the discussion, attention will be devoted exclusively to the relationship between 180° electron scattering and M1 transitions. The remarks will, of course, also be applicable, but to a lesser degree, to scattering at backward angles not too far from 180°. Two features of this relationship will be highlighted: (a) assuming certain approximations (cited below) only the transverse electric and magnetic components are non-zero at 180°, (b) of these, the transverse magnetic usually dominates if the excitation energy is not too high compared to the incident electron energy.

If we regard the electromagnetic interaction as that between the nuclear charges and currents and the virtual photons generated by the electron in its trajectory, the two components can be defined in terms of the polarizations of these virtual photons. As shown in the schematic diagram in Fig. 1, the longitudinal interaction results from those virtual photons polarized along the direction of the momentum transfer, $\mathbf{q}$, while the transverse interaction results from those polarized perpendicular to this direction.

The distinction between these components is clear in the expression for the cross section in the plane wave Born approximation (PWBA), where each term is either longitudinal or transverse. However, in the distorted wave expression (DWBA), interference terms dilute this distinction. Thus, for conceptual simplicity we will discuss the plane wave expression which for a given multipolarity and for the two components can be written as:

$$\frac{d\sigma_l}{d\Omega} = \frac{4\pi\alpha}{[(2L+1)!!]^2}\frac{q^{2L}}{p^2}B(CL,q)V_l(\theta), \tag{1}$$

$$\frac{d\sigma_t}{d\Omega} = \frac{4\pi\alpha(L+1)}{L[(2L+1)!!]^2}\frac{q^{2L}}{p^2}[B(EL,q)+B(ML,q)]V_t(\theta), \tag{2}$$

with

$$V_l = \frac{\cos^2(\theta/2)}{4\sin^4(\theta/2)}, \quad V_t = \frac{1+\sin^2(\theta/2)}{8\sin^4(\theta/2)}, \tag{3}$$

where α is the fine structure constant, q is the momentum transfer, p the incident electron momentum, and $\hbar = c = 1$. The expressions for V_l and V_t are valid in the approximation that $p \gg \omega$ and m, where ω is the excitation energy, and m the electron mass.[2] Here $B(CL,q)$, $B(EL,q)$, and $B(ML,q)$ are the reduced transition probabilities for longitudinal, transverse electric, and transverse magnetic interactions, respectively.

Inspection of Eq. (3) shows that at $\theta = 180°$, $V_l = 0$; and thus $d\sigma_l/d\Omega = 0$. This is the first important feature of 180° electron scattering: that only the transverse electric and magnetic components contribute to the cross section, subject to the above approximations.

The vanishing of the longitudinal component in the above equations may be visualized in terms of the conservation of helicity (Peterson, 1973; Rosen, 1973). If it is assumed that the electron energy is large enough and the electron spin is thus aligned or opposite to its momentum direction, then the conservation of helicity should be approximately valid. For helicity to be conserved in a 180° scattering as shown in Fig. 2, a spin-flip must

[1] For reviews of M1 transitions *per se*, see, for example, Hanna (1969) and Yoshida and Zamick (1972).

[2] When the electron mass is not ignored, $V_l \neq 0$ at 180° and the exact expressions [Eqs. (12) and (13) of Barber (1962)] must be used.

occur. Since the longitudinal interaction cannot cause a spin-flip, only the transverse electric and magnetic interactions will contribute under these conditions.

Of these two interactions, it can be shown by means of two arguments that, for a given multipolarity, the magnetic generally dominates in a 180° scattering, if the excitation energy is not too high (Barber *et al.*, 1963). The first of these arguments is based on the order of magnitude estimates of the PWBA cross sections involved. For example, using the independent particle model (Blatt and Weisskopf, 1952) and assuming the same initial and final state spins and the same transition radii for the two kinds of transitions, and $\omega = 10$ MeV and $q = 90$ MeV/c, a ratio of $\sigma(\mathrm{M1})/\sigma(\mathrm{E1}) \cong 16$ is obtained (Rosen, 1973).

That this dominance of the M1 cross section should prevail in 180° scattering is supported by another, somewhat more fundamental argument (Adler, 1968; 1973) which we start by setting down the expressions for the four components of the electron current due to the beam electrons. Assuming $p, p' \gg m$, then it can easily be shown that:

$$\begin{aligned} j_x &= u_f^\dagger \alpha_x u_i \cong -2i(pp'/4m^2)^{\frac{1}{2}} \chi_f^\dagger \sigma_y \chi_i, \\ j_y &= u_f^\dagger \alpha_y u_i \cong 2i(pp'/4m^2)^{\frac{1}{2}} \chi_f^\dagger \sigma_x \chi_i, \\ j_z &= u_f^\dagger \alpha_z u_i \ll j_x, j_y, \\ j_0 &= u_f^\dagger u_i \ll j_x, j_y, \end{aligned} \tag{4}$$

where p and p' are the incident and scattered electron momenta, respectively, and u_f, u_i and χ_f, χ_i are the 4 component and 2 component final and incident electron spin functions, respectively. Now j_x and j_y are only nonzero for a spin flip; and j_z and j_0, which are small relative to j_x and j_y, are neglected. Thus, if a spin flip occurs in the 180° scattering, we have

$$\mathbf{j} = (pp'/m^2)^{1/2} \exp(i|\mathbf{q}|z - iq_0 t) \begin{bmatrix} 1 \\ i \\ 0 \end{bmatrix}, \tag{5}$$

where the space-time part of the electron wavefunction has been included and the products of the spinors and Pauli matrices evaluated; and where $\mathbf{q}$ is the 3 momentum transfer, and q_0 is the zeroth component of the momentum transfer ($\approx\omega$, neglecting recoil). Note that Eq. (5) has been calculated for the case of initial spin in the direction of the incident momentum. Solving the reduced Maxwell equation

$$\Box^2 \mathbf{A} = \mathbf{j} \tag{6}$$

for the vector potential $\mathbf{A}$ we have:

$$\mathbf{A} = \frac{1}{\mathbf{q}^2 - q_0^2} (pp'/m^2)^{1/2} \exp(i|\mathbf{q}|z - iq_0 t) \begin{bmatrix} 1 \\ i \\ 0 \end{bmatrix}. \tag{7}$$

Now if the excitation energy ω is not too large then $|\mathbf{q}| \gg q_0$, and we can state:

$$\mathbf{E} = \dot{\mathbf{A}} \cong \frac{-iq_0}{\mathbf{q}^2} (pp'/m^2)^{1/2} \exp(i|\mathbf{q}|z - iq_0 t) \begin{bmatrix} 1 \\ i \\ 0 \end{bmatrix} \cong 0 \tag{8}$$

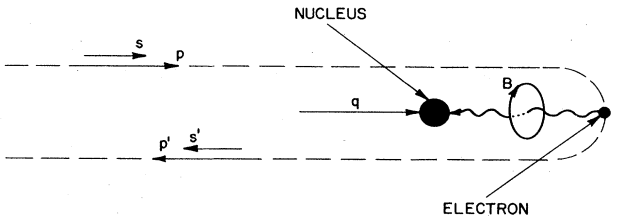

FIG. 2. The circular polarization of the virtual photon in a 180° electron spin-flip scattering. Left-hand circular polarization with respect to $\mathbf{q}$ obtains when the electron spin and momentum are aligned. The electron trajectory is shown for descriptive purposes and not intended to depict the actual trajectory [figure from Fagg (1973)].

and

$$\mathbf{B} = \nabla \times \mathbf{A} \cong \frac{i|\mathbf{q}|}{\mathbf{q}^2} (pp'/m^2)^{1/2} \exp(i|\mathbf{q}|z - iq_0 t) \begin{bmatrix} -i \\ 1 \\ 0 \end{bmatrix}. \tag{9}$$

Thus, under the conditions of the approximation used for these last two expressions, only $\mathbf{B}$ is nonzero, and the transition is magnetic. Since a spin flip is involved, the angular momentum change is 1. Thus assuming the lowest orbital angular momentum involves the strongest interaction (which is true at the low momentum transfers considered here), we see that an M1 transition will dominate. It should be remembered that the magnetic field expressed in Eq. (9) is that associated with a virtual photon, and not a real magnetic dipole photon which would have an accompanying electric field.

It needs to be stressed that Eqs. (8) and (9) are valid only when $|\mathbf{q}| \gg q_0 \approx \omega$ (if the recoil is not too great), which, incidentally is the same approximation under which Eqs. (3) are valid. When this is not the case and ω becomes comparable with $|\mathbf{q}|$, then the transverse electric field becomes effective. This feature of 180° scattering will be discussed further in Sec. IV.A.3.

Perhaps the most interesting feature of the result expressed in Eq. (9) is, as an inspection of the phases of the components shows, that $\mathbf{B}$ is circularly polarized. As mentioned earlier in calculating Eq. (5), the result in Eq. (9) is for the case when the electron spin is directed along the incident and scattered momenta. A little study of the relative phasing shows that the field in Eq. (9) is left-hand circularly polarized with respect to the direction of $\mathbf{q}$ as shown in Fig. 2. If the incident and scattered spins were aligned in a direction opposite to the corresponding momenta, $\mathbf{B}$ would be right-hand circularly polarized. This means that even with an unpolarized incident beam the nucleus in a 180° scattering has effectively been subjected to a nuclear alignment {for definition of nuclear alignment [see Fagg and Hanna (1959), p. 712]}.

B. Nuclear properties studied at backward angles

1. Plane wave Born approximation

In this subsection, we will confine our remarks on the study of nuclear properties to those determined by means of electron scattering at 180° only, using a PWBA analysis. A discussion of DWBA corrections to such PWBA

analyses as well as direct DWBA analysis itself will be given in the next subsection. From the measured values of the experimental cross sections at 180°, three nuclear properties can in principle be determined (assuming $q \lesssim 100$ MeV/c): XL, the multipolarity of the transition excited ($X = E$ or M); $R_{\rm tr}$, the transition radius; and Γ_0, the transition width to the ground-state. The value of the latter quantity can often provide useful restrictions on nuclear wave functions (e.g., see Sec. IV.A.1). The question of the physical significance of $R_{\rm tr}$ will be discussed in the next subsection.

The PWBA expression for transverse inelastic scattering cross section at 180° is:

$$\left(\frac{d\sigma}{d\Omega}\right)_{180^\circ} = \frac{\pi\alpha}{[(2L+1)!!]^2}\frac{L+1}{L}\frac{q^{2L}}{p^2}B(XL,q), \tag{10}$$

where L is the multipolarity, $X = E$ or M, q the momentum transfer, p the incident electron momentum, α the fine structure constant, and $B(XL, q)$ the reduced transition probability. Note that Eq. (10) is Eq. (2) for $\theta = 180°$, where $V_t = \frac{1}{4}$. Incidentally, it should be remembered that at 180°, one has $q = 2p - \omega$, where ω is the nuclear excitation energy; thus the only means of varying q is by varying the incident electron energy since other angles are not available in most 180° systems. The reduced transition probability $B(XL, q)$ can be expanded in terms of q and the transition radii R_{lX} ($l = 2, 4, 6, \cdots$), which for the magnetic multipolarities is given by (Rosen *et al.*, 1967):

$$B(ML,q) = B(ML,0)\left[1 - \frac{L+3}{L+1}\frac{(qR_{2M})^2}{2(2L+3)} + \frac{L+5}{L+1}\frac{(qR_{4M})^4}{8(2L+3)(2L+5)} - \cdots\right]^2, \tag{11}$$

where the first two transition radii R_{lM} are defined as (Rosen *et al.*, 1967):

$$R_{2M}{}^2 = \frac{L+1}{L+3}\frac{\langle J\|r^{L+2}\|J_0\rangle_m}{\langle J\|r^L\|J_0\rangle_m}, \tag{12}$$

$$R_{4M}{}^4 = \frac{L+1}{L+5}\frac{\langle J\|r^{L+4}\|J_0\rangle_m}{\langle J\|r^L\|J_0\rangle_m}. \tag{13}$$

Initial and final states are here denoted by their spins, J_0 and J, respectively. In Eqs. (12) and (13):

$$\langle J\|r^{L+l}\|J_0\rangle_m = \langle J\|\int d^3r[r^{L+l}\mathbf{j}\cdot\mathbf{Y}_{LL}(\hat{r}) + \boldsymbol{\mu}\cdot\nabla\times r^{L+l}\mathbf{Y}_{LL}(\hat{r})]\|J_0\rangle, \tag{14}$$

where $\mathbf{j}$ and $\boldsymbol{\mu}$ are the nuclear charge current and magnetization density, respectively.

The reduced transition probability for the electric multipolarities is given by:

$$q^2B(EL,q) = \lim_{q\to 0}[q^2B(EL,q)]\left[1 - \frac{L+3}{L+1}\frac{(qR_{2E})^2}{2(2L+3)} + \frac{L+5}{L+1}\frac{(qR_{4E})^4}{8(2L+3)(2L+5)} - \cdots\right]^2, \tag{15}$$

where the first two transition radii are:

$$R_{2E}{}^2 = \frac{L+1}{L+3}\frac{\langle J\|r^{L+2}\|J_0\rangle_{ej} - 2(2L+3)R_c{}^2\langle J\|r^L\|J_0\rangle_{e\mu}}{\langle J\|r^L\|J_0\rangle_{ej}}, \tag{16}$$

$$R_{4E}{}^4 = \frac{L+1}{L+5}\frac{\langle J\|r^{L+4}\|J_0\rangle_{ej} - 4(2L+5)R_c{}^2\langle J\|r^{L+2}\|J_0\rangle_{e\mu}}{\langle J\|r^L\|J_0\rangle_{ej}}, \tag{17}$$

where R_c is the charge radius of the nucleus. In Eqs. (16) and (17) the matrix elements due to nuclear charge currents and magnetization density, respectively, are:

$$\langle J\|r^{L+l}\|J_0\rangle_{ej} = R_c\langle J\|\int d^3r\mathbf{j}\cdot\nabla\times r^{L+l}\mathbf{Y}_{LL}(\hat{r})\|J_0\rangle, \tag{18}$$

and

$$\langle J\|r^{L+l}\|J_0\rangle_{e\mu} = R_c{}^{-1}\langle J\|\int d^3r r^{L+l}\boldsymbol{\mu}\cdot\mathbf{Y}_{LL}(\hat{r})\|J_0\rangle. \tag{19}$$

When the transition radius $R_{\rm tr}$ is referred to hereafter, it is taken as equal to R_{2M} or R_{2E} depending on the transition being discussed. Only the transverse electric and magnetic components of the cross section have been given above because of the considerations discussed in Sec. A.

In principle a truly model-independent analysis of experimental results using the above expressions is only possible when all of the R_{lX} are determined. Of course, this would mean accurately measuring cross section values at a large number of different values of the momentum transfer including very high ones. However, since the expansions in Eqs. (11) and (15) converge rapidly for low momentum transfers and the lighter nuclei (which have smaller values of R_{lX}; see below), in practice only a few measurements of the cross section at different momentum transfers are necessary for a virtually model-independent analysis. In general for heavier nuclei such an analysis, even though DWBA corrected, is not accurate and direct DWBA cross section calculations are then needed.

As an example of data reduction leading to values of XL, $R_{\rm tr}$, and Γ_0, we describe the nearly model-independent analysis presently used (Maruyama *et al.*, 1974) at NRL for light ($A \leq 40$) nuclei (subject to DWBA corrections discussed in the next subsection). Since thus far in the light nuclei at 180° and at low bombarding energies multipolarities of $L \geq 3$ have not been observed, only M1, M2, E1, and E2 transitions are considered in the multipolarity determination. Curves of cross section vs momentum transfer for all four multipolarities are then calculated using, for example, the generalized Helm model (Rosen *et al.*, 1967) and compared with the experimental curve.

With this technique usually unambiguous multipolarity assignments can be made, or at least some possibilities can be eliminated. An example of how this technique rather unambiguously assigns the 7.63-MeV transition in ^{22}Ne an M2 character is shown in Fig. 3, whereas in Fig. 4 an ambiguity is present in the 9.14 MeV transition which is either M1 or E2 in character. In cases such as the latter one theoretical arguments may often be used to resolve the ambiguity. For example, if the 9.14 MeV transition is assumed to be E2 and on this basis its transition width is calculated, this width turns out unreasonably larger than that of a shell model calculation (Wildenthal,

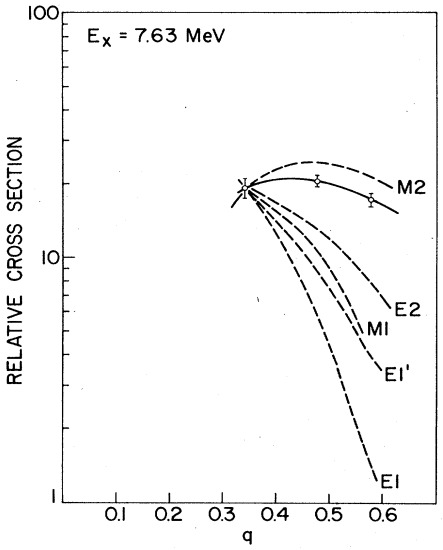

FIG. 3. Comparison of the experimental curve of cross section vs. q based on three data points with various generalized Helm model curves for the four multipolarity possibilities considered in the case of the 7.63 MeV transition in ^{22}Ne. The two curves E1 and E1′ represent the range of "reasonable" transition radii that were used.

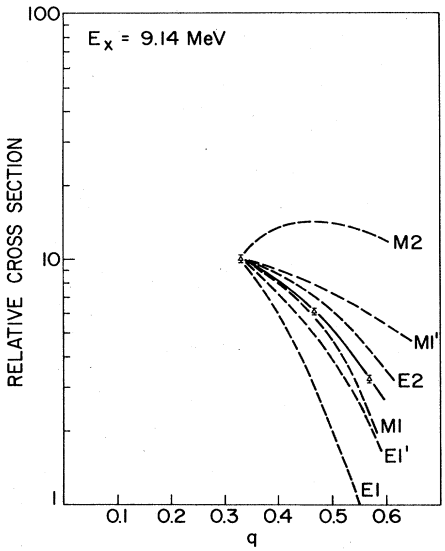

FIG. 4. Comparison of the experimental curve of cross section vs. q based on three data points with various Helm model curves for the four multipolarities considered in the case of the 9.14 MeV transition in ^{22}Ne. The two curves E1 and E1′ and the two, M1 and M1′, correspond to the ranges of "reasonable" transition radii that were used in each case.

1973). Accordingly an M1 assignment is the more probable for this transition.

Another feature of the generalized Helm model calculations that plays a strong role in the multipolarity determination is the preliminary transition radius used. This quantity according to the model is given in (Rosen *et al.*, 1967) by expressions (42b) and (43b) for electric and magnetic multipole transitions, respectively. It has effectively become an empirical rule that at least for the light nuclei ($A \leq 40$) the transition radius must be roughly equal to the ground state nuclear charge radius R_c. This can be seen from Fig. 5 which summarizes the data for light nuclei (Theissen, 1972) showing that for M1 transitions $R_{tr}/R_c = 1.09$.

The use of the Helm model for this phase of the analysis is a matter of simplicity and convenience. The resolution of any ambiguities that the Helm model approach cannot resolve, can, of course, always be attempted with a more model-independent approach using the expressions given above. In any event once the multipolarity is determined, then a best fit of the above expressions to the experimental cross section curve extrapolated to $q = 0$ is undertaken by varying the values of the transition radii in Eqs. (11) or (15). With this fitting procedure the final value of R_{tr} can be determined. Then using the value of the chosen cross section curve at $q = 0$, one can determine $B(XL,0)$. This quantity can in turn be used to determine Γ_0 from the relation:

$$\Gamma_0 = 8\pi \frac{L+1}{L} \frac{\omega^{2L+1}}{[(2L+1)!!]^2} \left(\frac{2J_0+1}{2J+1}\right) B(XL,\omega), \quad (20)$$

where $B(XL,\omega)$ can be found from Eqs. (11) or (15) by inserting $q = \omega$, the excitation energy.

The foregoing description of the analysis of 180° scattering data (subject to DWBA corrections discussed in the next subsection) leading to values XL, R_{tr}, and Γ_0 is obviously only one variation of several possible. However, it would seem that all would have to be initiated by trial multipolarities as well as fitting to determine R_{tr}. Obviously, since data are taken at only one angle (180°) as discussed here, occasional ambiguities in multipolarity assignment will occur, which are best resolved by taking additional data at more forward angles. Without DWBA corrections, such PWBA analysis procedures as the above are at present rarely used for nuclei with $Z > 6$, and if high accuracy is desired, corrections must be made even for the lightest of nuclei.

2. Distorted wave Born approximation

The Coulomb field of the nucleus distorts both the initial and final wave of the electron in a scattering.

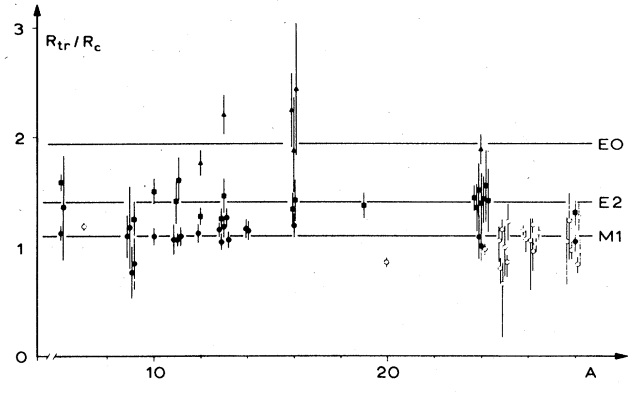

FIG. 5. Transition radii R_{tr} divided by ground state rms charge radius R_c as a function of mass number A. Of interest here is the M1 curve. Full symbols denote results from scattering <180°; open symbols denote results from 180° scattering [figure from Theissen (1971)].

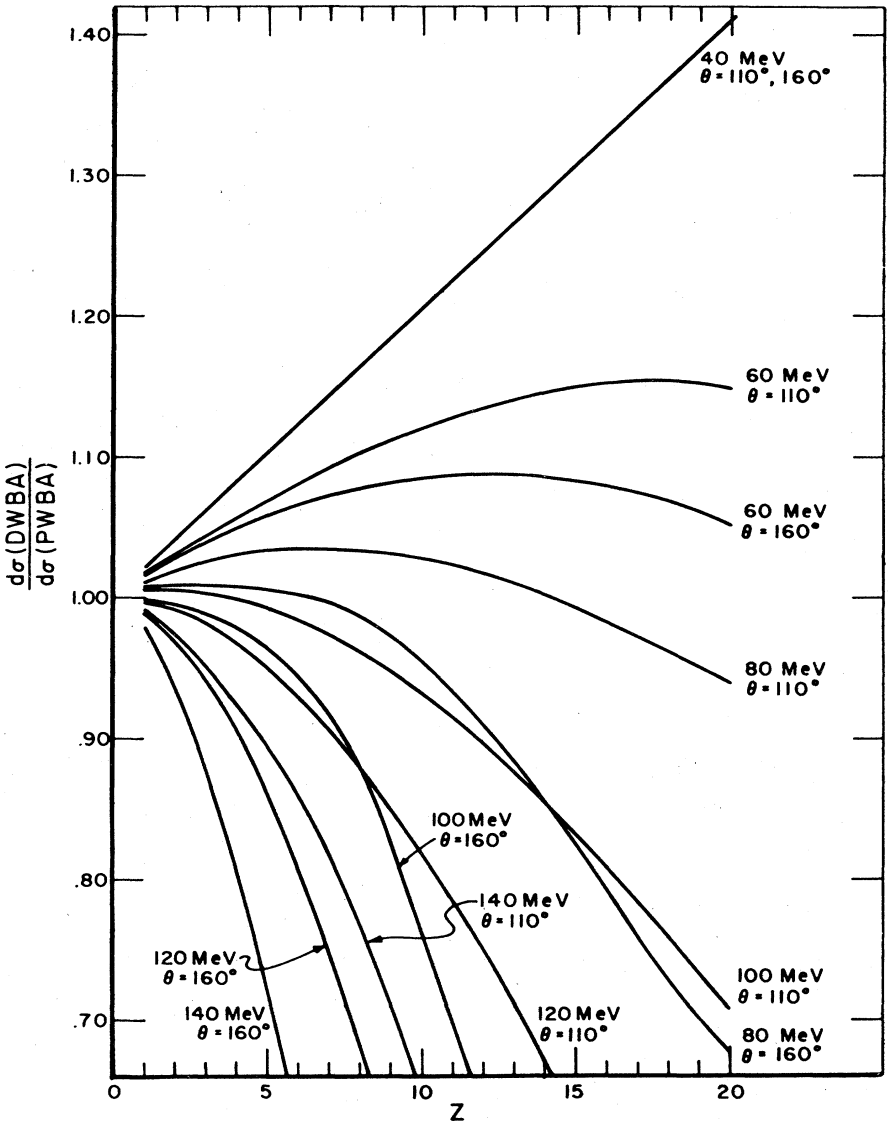

FIG. 6. The correction factor $f_c = (d\sigma/d\Omega)_{DWBA}/(d\sigma/d\Omega)_{PWBA}$ vs. Z, E_0, and θ for M1 electroexcitation at 15 MeV [figure from Chertok *et al.* (1970)].

Nuclear currents and magnetization densities also affect these waves but to an extent which does not yet justify correction in view of the accuracy of present-day measurements.

Two approaches have been used in taking into account Coulomb distortion effects. The first, an approximate method, is to calculate, usually by partial-wave analysis in the DWBA, cross section correction coefficients which can be applied to the experimental cross sections so that the corrected value can be related to PWBA expressions and analyzed accordingly. The second, an exact method, is to compare the experimental values with the appropriate DWBA calculation directly. The first method has the advantage of simplicity in that usually only elementary interpolations between tables of correction values need be made and that a PWBA analysis, which better highlights the nuclear properties involved, can be used. However, this method is inadvisable for use with heavier nuclei ($A \geq 40$), in which case the direct DWBA calculation must be used.

The approximate or correction method uses a distorted wave correction factor given by

$$f_c = (d\sigma/d\Omega)_{\mathrm{DWBA}}/(d\sigma/d\Omega)_{\mathrm{PWBA}}. \tag{21}$$

The experimental cross section is then divided by f_c

$$(d\sigma/d\Omega)_{\mathrm{PWBA}}{}^{\mathrm{exp}} = (d\sigma/d\Omega)^{\mathrm{exp}}/f_c \tag{22}$$

to give an "experimental PWBA" cross section which can be related to the theoretical PWBA expressions for analysis.

The principal problem encountered in the use of such a technique is performing it in a model-independent way. Essentially this problem reduces to separating the Coulomb distortion effects from the effects of the transition charge, current, and magnetization densities in the cross section. Roughly speaking model independence will be valid if the PWBA cross sections are equal in the momentum transfer range under study for the various models considered (Drechsel, 1968). Then the corresponding DWBA cross

sections as well as the corresponding f_c will coincide. Such a situation will generally prevail for low momentum transfers and $A \lesssim 40$ nuclei (Theissen, 1972).

The matter of model-independent correction factors for cross sections involving transverse transitions, in particular M1 transitions, is a somewhat more difficult problem than that for other transitions. Intimately associated with this problem is the question of the model-independent physical meaning of an M1 transition radius (Drechsel, 1967 and 1968) to be discussed below.

Using the Duke DUELS (Tuan *et al.*, 1968) program which considers magnetization resulting only from orbital nuclear currents and not from magnetization density, Chertok (Chertok and Johnson, 1969; Chertok, 1969; and Chertok *et al.*, 1970) has calculated values of f_c for M1 excitation cross sections with incident electron energy $E < 140$ MeV, and for nuclei with $Z \leq 20$. A correction factor linear with Z is found at $E = 40$ MeV; however, as the incident energy is increased there is a strong departure from linearity as is apparent in Fig. 6 which shows curves of f_c vs Z for various values of E and θ and for $\omega = 15$ MeV. It might be added that Chertok has also calculated with the same program M2 correction factors (Chertok *et al.*, 1970) again for low E and Z. These results along with M1 correction factors can be found in tables (Chertok *et al.*, 1970a).

The problem of the model dependence of f_c has been studied in some detail by Drechsel (1967 and 1968) who included in his calculation consideration of not only the nuclear orbital currents but also the nuclear magnetization. In conjunction with the study of f_c, the closely related problem of the model-independent physical meaning of the transition radius for M1 transitions is treated. It is pointed out that for longitudinal transitions there is a one-to-one correspondence between the moments of the transition charge density $\rho_L(r)$ and the expansion of the transition matrix element in terms of a transition radius [analogous to that given in Eqs. (11) and (15)]. In this case then the transition radius can have physical significance. However, for transverse transitions more than one moment of the transition current and magnetization densities can appear in a term of the matrix element expansion.

This fact is amplified by calculating the transition radius using several different models. Drechsel starts by regarding the M1 transition radius [given in Eq. (11) for $L = 1$] as merely a convenient expansion parameter. He thus expands the experimental form factor yielding:

$$F_{\text{exp}} = q^L \sum_{n=0}^{\infty} (-)^n \alpha_n{}^{\text{exp}} q^{2n}, \tag{23}$$

where $\alpha_n{}^{\text{exp}}$ is a general expansion parameter. Then the five different nuclear models given in Table I are considered, two of which involve nuclear currents only, and three of which involve nuclear magnetization only. Assuming the PWBA and that $\alpha_1{}^{\text{exp}}$ has been measured according to Eq. (23), the following values of transition radii are found from the models given in Table I:

$$\alpha_1{}^{\text{exp}} = \tfrac{1}{10} R_A{}^2 = \tfrac{1}{3} R_B{}^2 = \tfrac{1}{6} R_C{}^2 = \tfrac{1}{5} R_E{}^2. \tag{24}$$

TABLE I.[a] Drechsel current-magnetization models for model dependence tests in M1 transitions.[b]

Model	Current magnetization
A	$\mathbf{j} \sim \delta(R_A - r)\mathbf{Y}_{11\mu}{}^*$
B	$\mathbf{j} \sim re^{-(3r/r_B)}\mathbf{Y}_{11\mu}{}^*$
C	$\mathbf{m} \sim \delta(R_c - r)\mathbf{Y}_{10\mu}{}^*$
D	$\mathbf{m} \sim \delta(R_D - r)\mathbf{Y}_{12\mu}{}^*$
E	$\mathbf{m} \sim \delta(R_E - r) \times [(\frac{2}{3})^{\frac{1}{2}} \mathbf{Y}_{10\mu}{}^* + (\frac{1}{3})^{\frac{1}{2}} \mathbf{Y}_{12\mu}{}^*]$

[a] Table from Drechsel (1968).

[b] $\mathbf{j}$,$\mathbf{m}$,$\mathbf{Y}^*$ and μ are the nuclear current, nuclear magnetization, vector spherical harmonic, and magnetic quantum number, respectively.

This clearly calls into question the physical reality of M1 transition radii in terms of specifying in which region of the nucleus the transition takes place. However, in a model where, in the first few terms of the matrix element expansion, no more than one each current and magnetization moment appear in any one term, it may be meaningful to speak of two transition radii, one for current and one for magnetization, assuming, of course, that the model is physically applicable.

As a result of this study Drechsel suggests using an iterative procedure to determine a model-independent f_c at low momentum transfers. First, determine the first few $\alpha_n{}^{\text{exp}}$ in Eq. (23) by evaluating the experiment in the PWBA. Then find any current and/or magnetization density which gives the same values of, say, α_0, α_1, and α_2 (for low momentum transfers). Use these densities and calculate a correction factor. Apply the correction factor to the experimental cross section, then repeat the procedure. Convergence should occur rapidly.

As mentioned earlier, certainly for nuclei with $A > 40$ the correction factor approach must be abandoned and direct comparison with DWBA calculations must be undertaken. In fact this is more frequently becoming the case even with the light nuclei. The first such DWBA calculation that enjoyed any general use for electroexcitation of transverse magnetic transitions was that on which the Duke computer program DUELS (Tuan *et al.*, 1968) is based. This program treats the nuclear excitation through first-order perturbation theory, but treats the Coulomb effects on the electron waves with a partial-wave analysis. As previously noted, in its original version it only accounted for magnetization due to nuclear orbital currents and not to magnetization density.

More recently, there have been developed amended versions of the DUELS program (Dieperink, 1973; Lapikas *et al.*, 1973; Lee, 1974) which take into account nuclear magnetization as well as convection currents. Independently developed or developing computer programs useful for electroexcited M1 transitions (Drechsel, 1968), and magnetic transitions generally (Andresen, 1974) also exist.

C. Radiation tails and radiative corrections

The frequently cited advantage of the electron as a nuclear probe, namely its use of the weak, well-known electromagnetic interaction, is offset by one serious disadvantage, its small mass. Because of this, it easily undergoes scatterings which in turn usually generate radiation.

This results, not only in the broadening of any spectral peak produced by an elastic or inelastic scattering, but also in such peaks being accompanied by a low energy radiation tail. The latter effect means that any inelastic peak must ride on top of a background produced by the radiation tails of the elastic peak as well as all inelastic peaks corresponding to lower-energy nuclear excitations. At forward scattering angles the intensity of this tail background can be orders of magnitude larger than that of an inelastic peak under study. An advantage of 180° scattering is that generally these intensities are at least comparable.

Since only the aspects relevant to back angle scattering will be discussed here, no attempt will be made to discuss comprehensively radiation tails and the three principal radiative corrections. Excellent reviews and treatments of these phenomena are now available in the literature (Maximon and Isabelle, 1964; Maximon, 1969; Mo and Tsai, 1969; Überall, 1971). The distinction between the radiation tail and the most important radiative correction, the Schwinger correction, has been very lucidly discussed by Maximon (1969) and will only be capsulized here. The contributions to the radiation tail are defined as arising from those scatterings involving emission of photons of energy $k > \Delta E$ (defined as hard photons), where ΔE is an arbitrary incremental energy, usually of the order of the peak width at half-maximum. Specifically, ΔE is the energy difference between the electron energy of the peak (at maximum) and a lower arbitrary cutoff energy which serves to delimit the intensity of the peak and separate it from the tail.

The first of the radiative corrections, the Schwinger correction,[3] corrects for the loss to the area under the peak of those electrons degraded in energy as a result of emission of any number of real soft photons of energy $k < \Delta E$ as well as the emission and absorption of virtual photons of any energy. Clearly, the larger the value of ΔE that is used in the calculation of this correction, the smaller will be the correction. It should be noted that the distinction between correction and tail is not subscribed to by Mo and Tsai (1969), who prefer to assemble all such phenomena into the category of corrections.

The Schwinger correction deals with quantum electrodynamical effects occurring during the scattering under study whereas the second principal correction, the bremsstrahlung correction, corrects for effects due to small-angle scatterings from nuclei before and after this scattering. The third correction arises from ionization due to Landau straggling or multiple small-energy losses due to atomic ionization.

Two radiation tail calculations (Maximon and Isabelle, 1964; Ginsberg and Pratt, 1964) are presently most applicable to backward angle magnetic scattering; however, only the former gives inelastic as well as elastic tails. Each of these are PWBA calculations which consider magnetic as well as charge scattering and which direct particular attention to 180° scattering. A more recent calculation (Gargaro and Onley, 1971) is in DWBA but considers only elastic tails generated by charge scattering.

The features of such calculations related to 180° magnetic scattering to be discussed here are: (1) even for a spinless nucleus (where the charge scattering cross section essentially vanishes at 180°) there exists an elastic radiation tail due to charge scattering, (2) the presence of magnetic bremsstrahlung is more prominent at 180°. The first point becomes clear qualitatively when it is noted that events originally destined to be off-180° scatterings without bremsstrahlung emission, can become effectively 180° scatterings as a result of the recoil from bremsstrahlung emission. This is illustrated approximately by the radiation tail curve presented in Fig. 7 which is based on the rather simple expression which results (Peterson and Barber, 1962) when 180° is substituted into the PWBA expression (McCormick *et al.*, 1956) for a point nucleus in the approximation that the incident electron energy $E \gg m$, the electron mass. The essential dependence in this expression is given by:

$$d\sigma^2/d\Omega dE \sim (1 - \gamma - \gamma^{-1} + \gamma^{-2}), \tag{25}$$

where $\gamma = p'/p.$, the ratio of the scattered to incident electron momenta. It can be seen from Fig. 7 that even though an elastic peak is not present, a tail is.[4] An experimental verification of this feature of 180° elastic scattering can be seen in the ^{4}He spectrum shown in Fig. 23. Due to finite solid angle and small-angle target scattering effects, elastic peaks invariably appear in 180° scattering spectra for higher Z spinless nuclei. However, since charge scattering has a Z^2 dependence, the effect of interest here is well highlighted for a very light nucleus such as ^{4}He.

The second feature mentioned above, magnetic bremsstrahlung, was first treated by Ginsberg and Pratt (1964). At 180° the intensity of this bremsstrahlung is greatest near the elastic peak, tailing off with increasing excitation energy as shown in Fig. 8. Magnetic bresmsstrahlung was first observed experimentally (Peterson and Barber, 1962) in scattering from hydrogen, and is clearly visible near the elastic peak in the ^{3}He spectrum also presented in Fig. 23.

Perhaps the most pertinent aspect of the Schwinger correction of relevance here is answering the question of whether the correction as usually given for charge scattering is applicable to backward magnetic scattering. Arguments have been given (Rand *et al.*, 1966; Maximon, 1969) to show that the same correction is valid, and this has been confirmed by actual calculations (Maximon, 1970; Borie, 1970). It has been pointed out (Borie, 1970) that for charge scattering at back angles the anomalous magnetic moment of the electron modifies the Schwinger correction. The modification is essentially due to the fact that at 180° the approximation of neglecting the electron mass for charge scattering is no longer justified. However, this effect does not occur for magnetic scattering.

Concerning the remaining two corrections, bremsstrahlung and ionization, clearly the only unique consideration

[3] A particularly clear discussion of the Schwinger correction is given in Überall (1971).

[4] Actually, when the electron mass is taken into account (Motz *et al.*, 1964), a small elastic peak is indeed present.

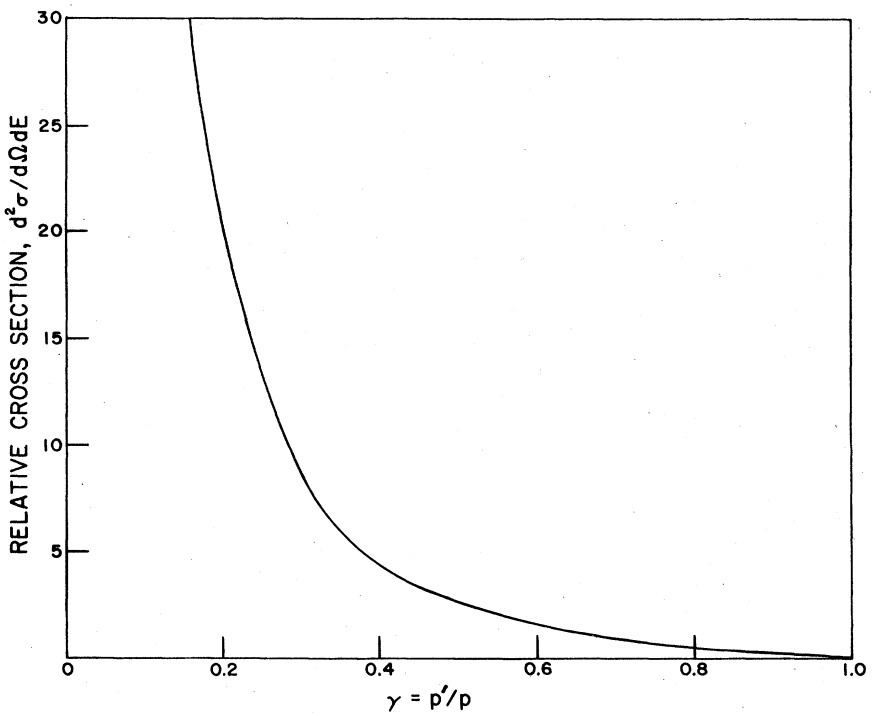

FIG. 7. Relative cross section for radiation tail for a spinless point nucleus vs. $\gamma = p'/p$, the ratio of the scattered to incident electron momenta. The curve follows a form used in Peterson and Barber (1962) of a relation derived in McCormick *et al.* (1956).

involved here is that reflection geometry obtains in backward scattering, the average distance a back-scattered electron travels being that of the full target thickness. This is so since an electron in 180° scattering can traverse target material up to twice the target thickness. Finally, the existence of some helpful articles on the details of radiative corrections (Mo and Tsai, 1969; Crannell, 1969; Isabelle and Berthot, 1970) in experimental data treatment should be noted as well as a recent report on target ionization loss (O'Brien *et al.*, 1974). A discussion (Rand, 1966) of target multiple scattering, finite solid angle, and finite angular and spatial incident beam effects in 180° scattering, and of curve-fitting (Chertok *et al.*, 1973) may also be helpful.

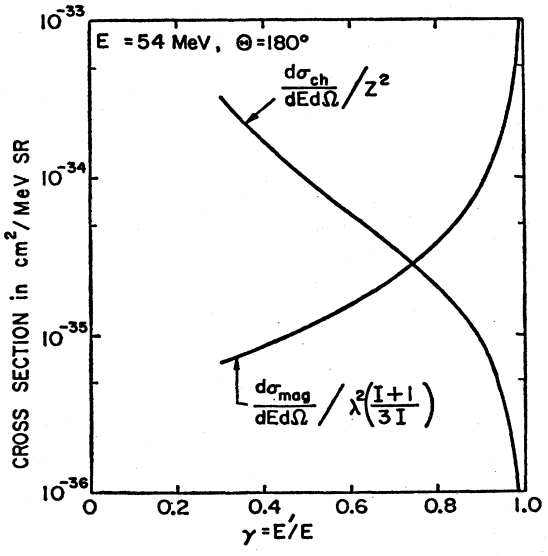

FIG. 8. Relative contributions to the radiative tail of the elastic peak from a point charge and a point magnetic moment in the limit $E,E' \gg 1, \theta = E^{-1}$ [figure from Ginsberg and Pratt (1964) and Goldemberg and Pratt (1966)].

III. REMARKS ON EXPERIMENTAL TECHNIQUES PECULIAR TO 180° SCATTERING

The most fundamental requirement of backward angle scattering, 180° scattering in particular, is that the incident and scattered beams must be separated. This necessitates the introduction of a separating or pretarget magnet of some form between the target and the spectrometer which measures the energy of the electrons scattered from the target. Thus as shown in Fig. 9(a) the beam from the electron Linac is deflected by the separating magnet to

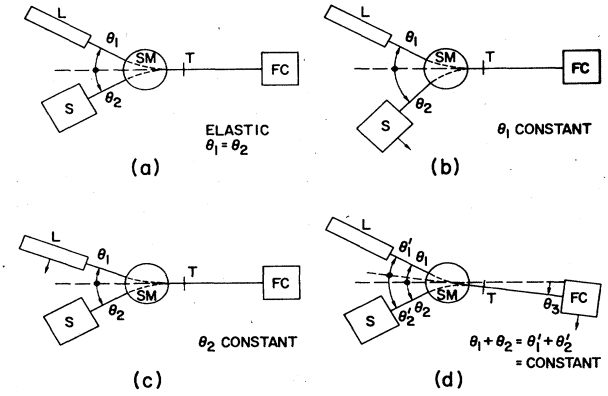

FIG. 9. Schematic diagram illustrating how 180° electron scattering can be performed for (a) elastic scattering, (b) inelastic scattering by rotating the spectrometer (θ_1 constant), (c) inelastic scattering by "rotating" the linac (θ_2 constant), (d) inelastic scattering by rotating the Faraday cup ($\theta_1 + \theta_2$ constant). The letters L, S, T, and FC stand for Linac, spectrometer, target, and Faraday cup, respectively.

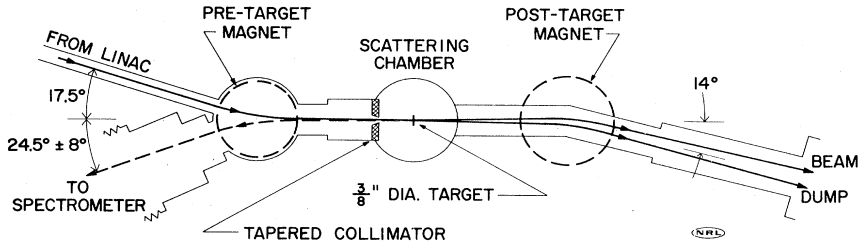

FIG. 10. The 180° electron scattering system at the Naval Research Laboratory (NRL) [figure from Bendel *et al.* (1968)].

the target. Generally the target is thin enough so that most of the beam passes on to the beam dump or Faraday cup, but those electrons which are elastically scattered at 180° follow the path indicated to the spectrometer.

However, the presence of the separating magnet immediately introduces the problem of how an inelastic spectrum is to be observed, i.e., how is a suitable energy range of inelastic electrons to be detected by the spectrometer. The geometry of the situation suggests three fundamental solutions (Bendel, 1972). First, the position of the spectrometer can be varied and the angle θ_1 kept constant as indicated in Fig. 9(b). Second, as shown in Fig. 9(c), the position of the Linac can be varied (in effect somehow) and θ_2 kept constant. Third, the position of the Faraday cup can be varied (variation of θ_3) and $\theta_1 + \theta_2$ kept constant as depicted in Fig. 9(d).

The presence of the separating magnet additionally generates other considerations some of which will be discussed. Perhaps the most important of these is that the object distance between the target and spectrometer must be increased beyond what it would be in more forward angle scattering by at least the path length used in traversing the separating magnet. This, of course, concurrently leads to a shorter spectrometer image distance with the result that often the effect of the spectrometer fringe field on the detectors in the focal plane, which is then closer to this field, must be dealt with. The increased object distance also results in a decreased spectrometer solid angle.

Another consideration arises in the use of the first and third 180° inelastic scattering techniques shown in Figs. 9(b) and 9(d), respectively. In both of these cases the angle between the spectrometer and beam line through the target is varied in taking an inelastic spectrum. This results in the complication that the solid angle acceptance of the separating magnet-spectrometer combination will vary with the inelastic electron energy.

Other considerations arise regardless of the 180° technique used in Fig. 9. For example, the problem of trapping with minimum background production those electrons that pass through the target (the post-target beam is actually, of course, a scattered beam with a strong predominance in the forward direction) is especially important in 180° scattering. Thus, the use of such devices as large quadrupoles, post-target bending magnets, and appropriately placed apertures are often needed to minimize the number of electrons which "backstream" from the Faraday cup into the spectrometer and thus mask the intensity observed from the target.

Also, since an incident electron which undergoes a 180° scattering in the target may traverse an amount of target material from zero to twice the target thickness, thinner targets than used in more forward angle scattering are often needed to achieve a desired resolution (Rand, 1972). Unfortunately this requirement occurs at the very angle where cross sections are generally the smallest and counting rate statistics are already a problem. It has been suggested that the target thickness could be compensated for by the introduction of a properly phased accelerating waveguide between the target and separating magnet (Rand, 1972).

Finally, the technique of relative cross section determination often used in more forward angle scattering involving comparison of the intensity of an inelastic peak with that of the corresponding elastic peak is usually not valid for the magnetic transitions observed at 180°. This is because, except for the very lightest nuclei, the experimentally observed elastic peak does not arise primarily from magnetic scattering, but from charge scattering produced by multiple scattering in the target and effects of finite solid angle and beam cross section. Therefore, certainly for nuclei with $A > 7$, either absolute measurements are made or comparison is made with a well-known transition such as the 15.11 MeV transition in ^{12}C. Many other problems unique to 180° must be dealt with; in the foregoing we have only mentioned those considered most important.

All of the 180° scattering facilities thus far in operation have basically used the technique shown in Fig. 9(b). The earliest such system operated at Stanford (Peterson, 1962; Peterson and Barber, 1962; Edge and Peterson, 1962) used a rectangular separating magnet. A system using a circular magnet as proposed by de Vries (1963) was designed and described in detail by Rand (1966), and was also used at Stanford. Such a system has since found some use at Orsay (Proca, 1966; Ganichot *et al.*, 1968; Ganichot *et al.*, 1972) and extensive current use at NRL (Bendel *et al.*, 1968) and Amsterdam (Van Niftrik *et al.*, 1971). Although the NRL system shown in Fig. 10 is typical, the most sophisticated system presently in operation is that at Amsterdam, shown in Fig. 11. In both systems, consistent with Fig. 9(b), a spectrum is obtained by rotating the spectrometer about the center of the separating magnet (not the target) in conjunction with setting the spectrometer field correspondingly. Also common to both systems is the use of an aperture between the target and separating magnet to absorb the backstreaming electrons scattered from the Faraday cup or beam dump, thus preventing their entry into the spectrometer.

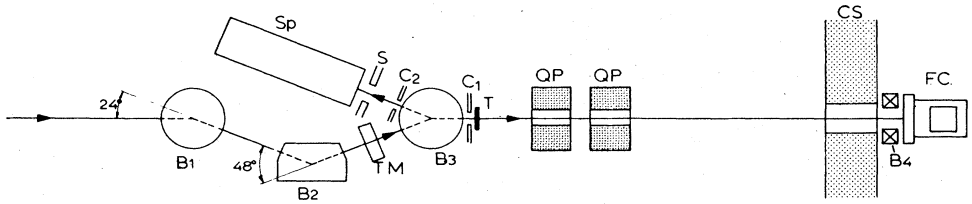

FIG. 11. The 180° electron scattering system at IKO Amsterdam. B1, B2, and B3 are the magnets of the 3-magnet pretarget array. Sp and S are the spectrometer and spectrometer slit, respectively. TM and T are the current monitor and target, respectively. C1 and C2 are lead collimaters. The *QP*'s and CS are the quadrupoles and cement wall, respectively. FC and B4 are the Faraday cup and Faraday cup trapping magnetic, respectively [figure from Van Niftrik *et al.* (1971)].

However, at NRL a post-target magnet is introduced between the target and beam dump (only ~1.2 m. apart due to space limitations) in order to deflect electrons emerging from the dump away from the target and pretarget (separating) magnet. A more satisfactory system is used by the Amsterdam group who are able to place the Faraday cup 6 m from the target through the use of two large quadrupole magnets which focus the scattered cone from the target into the cup.

There are two especially attractive characteristics of the Amsterdam system, each related to accommodation of scattering at more forward angles. The first pertains to the array of three magnets (see Fig. 11), including the separating magnet, that are upstream of the target. After the spectrometer is rotated out of the way, this array, mounted on tracks that are parallel to the general beam direction, can be slid upstream so that the target can also be moved upstream to the spectrometer center of rotation. Therefore, conventional scattering at forward angles can be accommodated by deactivating the three magnets and installing a beam pipe directly across the array. This accommodation is made possible by the 3-magnet array because the beam direction is not changed by the separating magnet as in single-magnet systems, e.g., NRL. The other attractive feature of the Amsterdam system is that it accommodates backward scattering at angles in the vicinity of 180°. By laterally displacing the incident beam, a scattering angle different from 180° can be obtained. With the recent addition of an enlarged vacuum chamber for the 3-magnet array a range from about 170°–180° can be covered.

Another variation of this method (Rand, 1966) involved displacement of the target and separating magnet jointly as is possible in the revised Stanford system (Rand, 1966) as shown in Fig. 12. For the angular variations near 180° the beam ditching magnet or post-target magnet is also movable jointly with the target and separating magnet along radial tracks. More forward angles can also be accommodated and the beam monitor calibrated by moving these three pieces entirely out of the way.

As indicated earlier, the 180° scattering system which have either been in operation or are presently in operation all use rotation of the spectrometer about the center of the separating magnet. The primary disadvantage of this method is the resulting variation of the solid angle with the spectrometer rotation angle (or scattered electron energy).

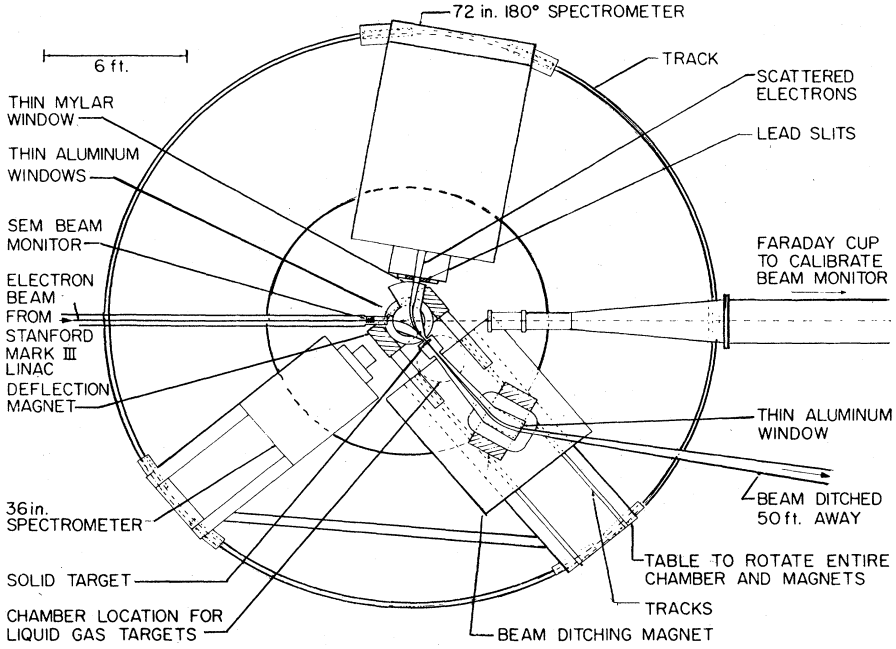

FIG. 12. The 180° electron scattering system designed at Stanford by Rand. The 36 in. (apparently used for intensity normalization) and 72 in. spectrometers and the target-beam ditching magnet assembly are all rotatable about the center of the separating magnet. The beam ditching magnet can also be moved radially [figure from Rand, 1966)].

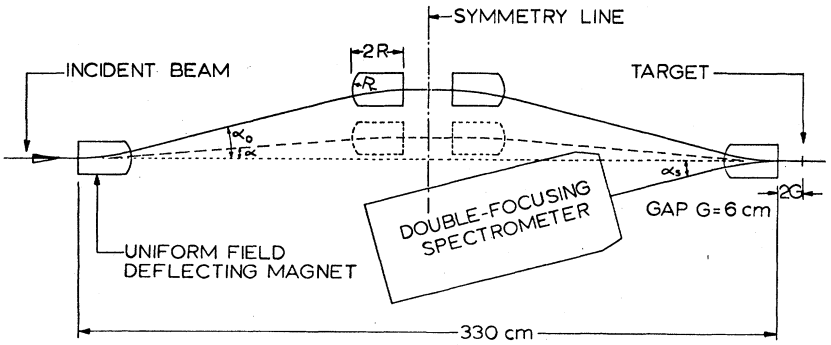

FIG. 13. The 4-magnet system for 180° electron scattering suggested by Peterson. The elastic scattering trajectory (where $\alpha_0 = \alpha_s$) is shown with solid lines and an inelastic trajectory at $\frac{1}{3}$ the incident momentum with the dotted lines [figure from Peterson (1968)].

There are at least three systems proposed to overcome the handicap of a variable solid angle. The one that has been taken most seriously is that shown in Fig. 13 (Peterson, 1968) where the spectrometer remains fixed and four identical pre-target magnets with identical fields are used [consistent with Fig. 9(c) where the linac is effectively "moved"]. At the field setting in the four magnets which renders the incident and scattered beam angles equal at the fourth magnet, the spectrometer observes elastically scattered electrons. An inelastic spectrum is then obtained by progressively decreasing the fields of the four magnets (as well as the spectrometer field proportionately) which in turn decreases the incident beam angle at the fourth magnet while the scattered beam angle, of course, remains constant. This system has the beauty of simplicity and economy in that the same field is maintained in each magnet.

An obvious variation of this scheme is to replace the middle two magnets with one. This has the disadvantage of relinquishing two pole edges which could be useful in making trajectory corrections. However, a compelling reason for breaking the symmetry of the 4-magnet array is that, more often than not, the fourth magnet (closest to the spectrometer) must be designed to integrate with the characteristics of the spectrometer, which usually renders the use of four identical magnets unfeasible. Other systems which maintain a constant solid angle have also been suggested by Bergstrom (1967) who used a principle of magnet design due to Koerts (1964) and by Leconte (1967).

Perhaps the most important concern in recent design of 180° systems is the effect of the pre-target magnet or magnets on operation in the so-called "dispersion matching" or "energy loss" mode. In this technique the dispersion of the last one or two magnets of the beam handling system is matched at the target with spectrometer dispersion. Under these conditions an elastically scattered electron from any position in the target in the dispersion range will be focussed at the same point in the spectrometer focal plane. However, one which suffers an inelastic collision in the target will focus at a different point. Hence also the name "energy loss." The clear advantage of such a system is that a much larger (up to the order of 100 larger) momentum bin of electrons from the Linac can be used in the electron scattering study, making it possible to take full advantage of the inherent resolution of the spectrometer. A disadvantage is that most beam handling systems disperse in a horizontal plane, whereas most spectrometers are mounted with their pole faces in a vertical plane. Thus, either special beam handling magnets must be introduced to disperse the beam vertically, as at Mainz and NBS, or the dispersion plane must be rotated to the vertical, e.g., by using five quadrupoles (Kowalski and Enge, 1972), as at Darmstadt and MIT.

Obviously the problems encountered in realizing such a refined system are formidable enough without the introduction of the pretarget magnet or magnets used in 180° scattering. Such magnets could have the effect of distorting the dispersion desired at the target. This problem has been investigated (Peterson and Vetter, 1974) using the TRANSPORT code in the design of the proposed 4-magnet 180° scattering system for the Bates-M.I.T. Linac. The conclusion, as of this writing, is that, in second order, due to vertical focussing effects, a loss in momentum resolution of about two parts in 10^{-4} does occur by the time the scattered beam reaches the spectrometer (M.I.T. spectrometer). Thus, relatively high resolution studies at 180° in the energy loss mode should be possible.

A final remark can be made concerning the technique of studying gaseous targets at 180° which is characterized by an especially simple cylindrical geometry. The gas chamber is enclosed by thin entrance and exit foils and is surrounded by a liquid nitrogen (or other coolant) cooling envelope which makes possible a target density gain of as much as a factor of three (Fagg *et al.*, 1970; Jones, 1974).

IV. DISCUSSION OF EXPERIMENTAL RESULTS

A. Self-conjugate nuclei

1. Theoretical preliminaries—sum rules

We deal with the self-conjugate nuclei separately, and give some prefatory theoretical remarks concerning them because there are characteristics of the M1 transitions in these nuclei which set them apart from other nuclei. The mechanism more often responsible for the strongest M1 transitions in such nuclei, indeed in nuclei generally, is the spin-flip mechanism. Its relative strength can be most easily theoretically demonstrated in the case of the self-conjugate nuclei.

We start with the general expression for an M1 transition matrix element between states a and b (Morpurgo,

1958)

$$\langle a|\sum_{i=1}^{A}\left\{\mathbf{L}_i\left(\frac{1+\tau_{3i}}{2}\right)+\mu_p\boldsymbol{\sigma}_i\left(\frac{1+\tau_{3i}}{2}\right)+\mu_n\boldsymbol{\sigma}_i\left(\frac{1-\tau_{3i}}{2}\right)\right\}|b\rangle, \tag{26}$$

where $\mathbf{L}_i$, $\boldsymbol{\sigma}_i$, and τ_{3i} are the orbital angular momentum, spin, and isospin operators of the ith nucleon, respectively, and μ_p and μ_n are the proton and neutron magnetic moments, respectively. Eq. (26) is valid in the limit $q\rightarrow\omega$, and thus should still be useful at low momentum transfers. Rearranging terms and adding and subtracting $\frac{1}{2}\boldsymbol{\sigma}_i$ inside the sum we have:

$$\tfrac{1}{2}\langle a|\sum_{i=1}^{A}[\mathbf{L}_i+\tfrac{1}{2}\boldsymbol{\sigma}_i]|b\rangle+\tfrac{1}{2}\langle a|\sum_{i=1}^{A}(\mu_p+\mu_n-\tfrac{1}{2})\boldsymbol{\sigma}_i|b\rangle+\tfrac{1}{2}\langle a|\sum_{i=1}^{A}\tau_{3i}\{\mathbf{L}_i+(\mu_p-\mu_n)\boldsymbol{\sigma}_i\}|b\rangle. \tag{27}$$

The first two terms of Eq. (27) constitute the isoscalar ($\Delta T=0$) part of the transition, while the third term with the τ_{3i} operator is the isovector ($\Delta T=1$) part. However, the first term is the matrix element of $\mathbf{J}=\sum_{i=1}^{A}(\mathbf{L}_i+\frac{1}{2}\boldsymbol{\sigma}_i)$ which vanishes due to the orthogonality of the two states (both being eigenstates of $\mathbf{J}$), so that only the second term gives the strength of the isoscalar transition. Since the $(\mu_p-\mu_n)$ term (the spin-flip term) of the isovector matrix element determines its order of magnitude, to compare the isoscalar and isovector strengths we can use

$$\frac{\mu_p+\mu_n-\frac{1}{2}}{\mu_p-\mu_n}=\frac{0.38}{4.7}. \tag{28}$$

When this ratio is squared, an intensity ratio $\sim 10^{-2}$ results. Here we have shown the general dominance of the spin-flip transition as well as outlined the derivation of the Morpurgo selection rule (Morpurgo, 1958). However, spin-flip transitions do not invariably dominate even in the self-conjugate nuclei, since orbital recoupling can in some instances dominate (e.g., ^{20}Ne; Sec. A.3 below).

From the foregoing (Morpurgo's rule) we see that $\Delta T=0$, M1 transitions in self-conjugate (ground state $T=0$) nuclei are strongly inhibited. Two results are evident: (1) there is a strong limitation in the number of M1 transitions experimentally observable in these nuclei, and (2) the remaining transitions, those with $\Delta T=1$, are to relatively high energy states ($\gtrsim 10$ MeV) which are analogs of low-lying states in neighboring ($\Delta T_3=\pm 1$) nuclei.

The number of $\Delta T=1$ transitions experimentally observed is, however, even further limited as a result of effects in the self-conjugate $4N$ and $4N+2$ nuclei studied by Kurath (1963). Using the shell model with spin-orbit coupling and central force two-body interactions, he showed that most of the M1 transition strength in the self-conjugate nuclei of the p-shell is concentrated in the lowest few $\Delta T=1$ transitions. Starting with the ground-state expectation value of the double commutator of his Hamiltonian with the z-component of the magnetic dipole operator, he also derived an M1 sum rule

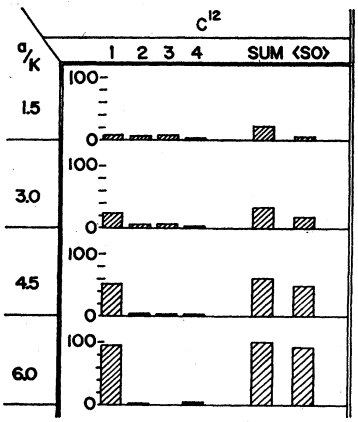

FIG. 14. Contribution of the four lowest $\Delta T=1$, M1 transitions in ^{12}C to the energy-weighted sum rule, their sum, and the ground-state expectation value of the spin-orbit term for different values of a/K (see text) [figure from Kurath (1963)].

$$\sum_k \omega_k B(\mathrm{M1})_k \cong -a(\mu_n-\mu_p+\tfrac{1}{2})^2\langle g|\sum_i \mathbf{l}_i\cdot\mathbf{s}_i|g\rangle, \tag{29}$$

where $B(\mathrm{M1})_k$ and ω_k are the reduced transition probability to, and excitation energy of, the kth level, respectively.

As an example of the concentration of the M1 strength into the lowest few $\Delta T=1$ transitions, Kurath calculated the $B(\mathrm{M1})_k$ for the lowest four $\Delta T=1$, M1 transitions in ^{12}C as shown in Fig. 14. This is done for four different values of a/K, where K is a representative integral of the two-body interaction. The sum of the four transition probabilities is also shown as well as the value of the rhs of Eq. (29). Particularly for values of $a/K=4.5$ and 6.0, the concentration of strength into the lowest $T=1$ level is apparent. Also evident is the fact that the ground-state expectation value of the spin–orbit coupling nearly equals this sum, justifying the assumption in his calculation that the two-body interaction term in his Hamiltonian does not significantly contribute. It is interesting to note (Überall, 1971) that the M1 strength is concentrated into the lower levels in contrast to the E1 giant dipole case where concentration is generally observed into the highest levels (Blatt and Weisskopf, 1952).

Kurath also extrapolates the use of Eq. (29) to the s–d shell, where, in some of the early experimental tests of the rule a version of the rule somewhat more useful to experimentalists is used (Kuehne *et al.*, 1967)[5]:

$$\sum_k\left[\frac{\Gamma_{0k}(\mathrm{M1})}{3.259\ \mathrm{eV}}\right]\left(\frac{10\ \mathrm{MeV}}{\omega_k}\right)^2=-\left(\frac{a}{2\ \mathrm{MeV}}\right)\langle g|\sum_i \mathbf{l}_i\cdot\mathbf{s}_i|g\rangle, \tag{30}$$

where Γ_{0k} is the transition width in electron volts for the transition from the kth level to the ground state. Since the M1 transition strength is usually concentrated into a very few $\Delta T=1$ transitions, the sum of the lhs of

[5] Dr.W. Bendel notes a 4% error in the value (3.395) given by Kuehne *et al.* (1967) for the denominator of the first factor of Eq. (30).

Eq. (30) is easy to measure. Thus, using a reasonable value of the parameter "a" such as indicated for the s–d shell from the $\mathbf{l}\cdot\mathbf{s}$ separation energy given by the 5.08 MeV state in ^{17}O, the ground state $\mathbf{l}\cdot\mathbf{s}$ coupling expectation value ($\langle\sum l\cdot s\rangle$, hereafter) can be determined. This value can then be used to place some restriction on the ground state wave function. This restriction often takes the form of a limitation on the possible ground state shapes a nucleus can assume as will be discussed below.

For a spherically symmetric nucleus in the simple shell model the ground state wavefunction $|g\rangle$ is an eigenfunction of the $\mathbf{l}\cdot\mathbf{s}$ operator and the eigenvalue is given by

$$\mathbf{l}\cdot\mathbf{s} = \tfrac{1}{2}[j(j+1) - l(l+1) - s(s+1)], \qquad (31)$$

where j, l, and s are the total, orbital, and spin angular momentum quantum numbers, respectively, of a given nucleon. Using Eq. (31) one can obtain an approximate idea of the expected pattern of total M1 strength among the self-conjugate nuclei in the s–d shell. As a specific example, to calculate the sum in ^{20}Ne where, in the shell model, the $d_{5/2}$ level is being filled, one obtains $\mathbf{l}\cdot\mathbf{s} = 1$ in Eq. (31). This is the value for one nucleon; since there are four nucleons in this subshell for ^{20}Ne, $\langle\sum l\cdot s\rangle = 4$. Proceeding accordingly with the other self-conjugate nuclei in the shell we find that $\langle\sum l\cdot s\rangle$ rises to a maximum of 12 at ^{28}Si and ^{32}S, then decreases to 6 at ^{36}Ar. Of course, zero is obtained for ^{16}O and ^{40}Ca.

Since the s–d shell nuclei are in general deformed, a more sensitive indication of how the M1 strength sum varies among these nuclei can be obtained by using the Nilsson model (Nilsson, 1955). Nilsson gives tables of deformed wavefunctions from which the value of $\langle\sum l\cdot s\rangle$ as a function of the deformation parameter η can be determined. An example of such a curve and the information it can give about ground state nuclear shapes, e.g., in ^{20}Ne, is shown in Fig. 20 and is discussed in Sec. A.3 below. Note that the maximum value of this curve is 4, equal to that given above for a spherical shape.

Just as in the Nilsson model, configuration mixing will tend to decrease the sum strengths in nuclei based on the pure independent particle shell model. The amount of this decrease can be related to the nucleon occupation numbers. Using the projected Hartree-Fock method, occupation numbers in the even s–d shell nuclei have been calculated (Castel *et al.*, 1970) and compared with experimental numbers using French's sum rule (French and McFarlane, 1961). Castel *et al.* also use their calculated occupation numbers to calculate in turn $\langle\sum l\cdot s\rangle$ using Kurath's sum rule, and find good agreement with the photon scattering results (Kuehne *et al.*, 1967) for M1 strengths in ^{24}Mg and ^{28}Si.

Other applicable sum rules exist. Pham (1972; 1972a; 1973) shows that $\Delta T = 1$, M1 transitions in self-conjugate nuclei result from symmetry breaking of $SU(4)$, and gives sum rules for the $4N$ and $4N + 2$ nuclei. Kurath (1972) in a study of triaxial shapes in s–d shell nuclei, gives a closure sum rule in the adiabatic model.

2. The deuteron

The deuteron is the most fundamental of all self-conjugate nuclei. In back angle scattering, it can be excited via the pure spin-flip $\Delta T = 1$ transition from the $^3S_1$ ground state to the $^1S_0$ state at breakup threshold. A visual idea of the strength of this spin-flip transition compared to that of the elastic scattering can be seen in the 180° scattering spectrum shown in Fig. 15 (Jones and Chertok, 1968).

Early Stanford experiments at 180° (Peterson and Barber, 1962; Barber *et al.*, 1963; Goldemberg and Schaerf, 1966) gave results which have been compared with varied success to applicable theories (Jankus, 1956; Durand, 1961). However, more recent measurements (Ganichot *et al.*, 1972) at 180° and at several incident electron energies below 280 MeV have shown essential agreement with the theories of Jankus and Durand.

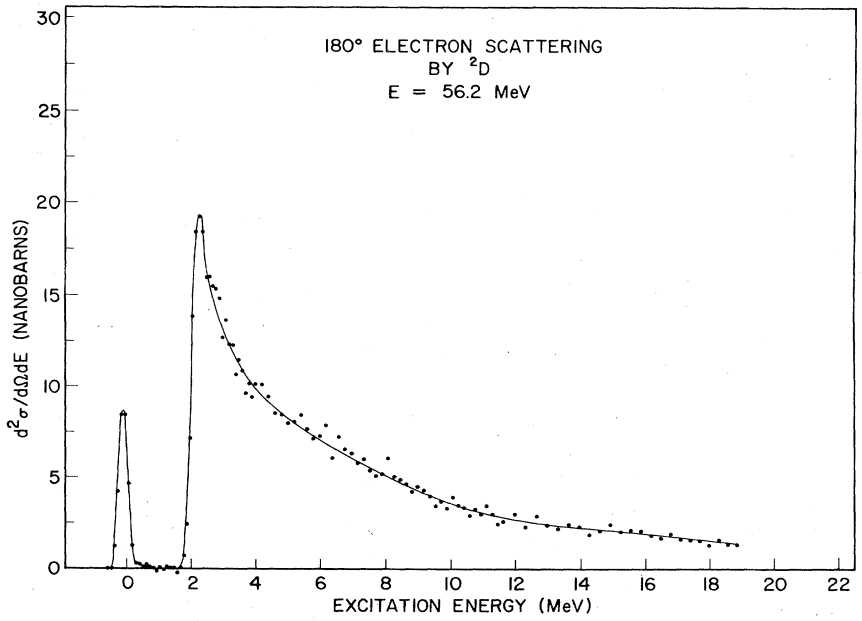

FIG. 15. Spectrum of 56.2 MeV electrons scattered at 180° from deuterium gas [figure from Jones and Chertok (1968)].

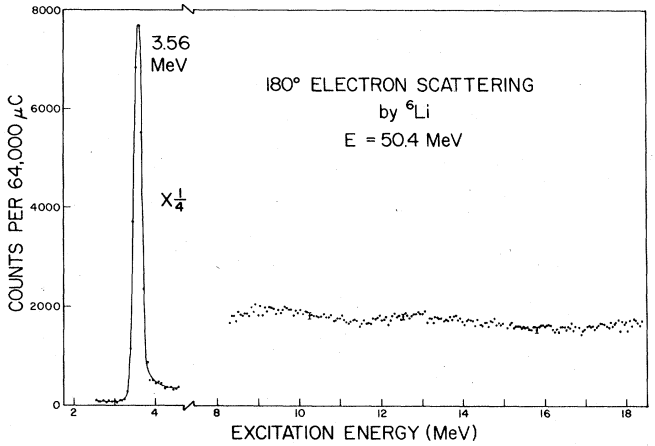

FIG. 16. Spectrum of 50.4 MeV electrons scattered at 180° from ^{6}Li. The peak at the left is due to the M1 transition at 3.56 MeV [figure from Fagg *et al.* (1973)].

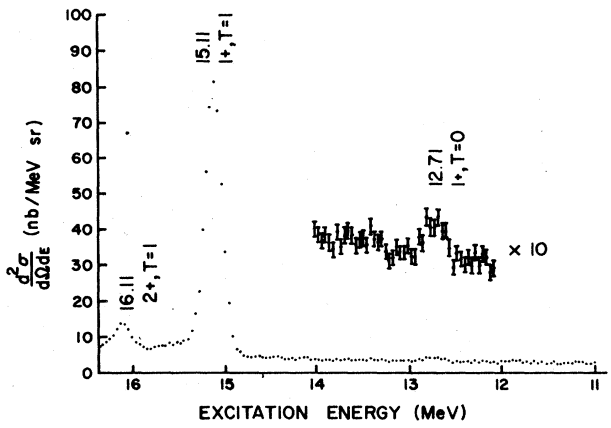

FIG. 17. Spectrum of 50.5 MeV electrons scattered at 180° from ^{12}C. The region around the 12.7 MeV peak has been enlarged by a factor of 10 [figure from Cecil *et al.* (1974)].

Especially since Bosco *et al.* (1964) have emphasized their importance, the use of 180° inelastic scattering from deuterium to examine the role of exchange currents has been a motivation for these experiments. Further incentive has been furnished by concurrent calculations of the exchange effects (Adler and Drell, 1964; Adler, 1966; and Blankenbecler and Gunion, 1971). However, meson current contributions increase with increasing q (Überall, 1971). Therefore, although more accurate low-q 180° inelastic experiments on the deuteron would be most useful, the preponderant recent interest has been in the work at higher values of q. Nevertheless, relatively recent work (Hadjimichael, 1973) covering the low-q region shows that meson exchange effects are more observable in the polarization of the break-up proton and neutron. On the other hand, Smirnov and Trubnikov (1974) calculate the 180° inelastic cross section taking into account final state interaction, but not meson exchange.

3. *p*- and *sd*-shell nuclei

The experimental results on the self-conjugate nuclei in the p- and sd-shells at least through ^{28}Si amply support Kurath's predictions (Kurath, 1963) as to the concentration of strength for $\Delta T = 1$, M1 transitions. In the p-shell this is exhibited in the transition at 3.56 MeV in ^{6}Li,[6] at 7.48 MeV in ^{10}B,[7] at 15.11 MeV in ^{12}C,[8] and at 9.17 and 10.43 MeV in ^{14}N.[9] Examples of spectra which illustrate this strength concentration in ^{6}Li and ^{12}C are presented in Figs. 16 and 17, respectively. In each case the dominant inelastic peak is considerably more intense than the elastic peak not shown.

In ^{6}Li some additional strength is observed at 5.36 MeV (Hutcheon *et al.*, 1970). A study using an intermediate coupling model (Neuhausen and Hutcheon, 1971) concludes that the 3.56 MeV transition is almost pure M1 spin-flip, 96% of the strength coming from the $^{3}S_1$–$^{1}S_0$ component of the transition. In this connection the transitions cited above for the odd–odd self-conjugate nuclei exhaust about 90%, 50%, and 90% of the M1 sum strength in ^{6}Li, ^{10}B, and ^{14}N, respectively (Hanna, 1974).

The classic M1, $\Delta T = 1$ transition at 15.11 MeV in ^{12}C often serves as a reference for relative measurements on transitions in other nuclei and consequently has been the subject of increasingly more accurate measurements. An Amsterdam-Darmstadt collaboration recently found $\Gamma_0 = 35.74 \pm 0.86$ eV (de Vries, 1972; Spamer *et al.*, 1972); this was later supported by the American University–NBS result, $\Gamma_0 = 37.0 \pm 1.1$ eV (Chertok *et al.*, 1973).

The electroexcitation of some of the M1 transitions in the p-shell self-conjugate nuclei have also been of interest for other reasons than strength concentration. For example, an experiment on ^{6}Li (Fagg *et al.*, 1973; Cardman *et al.*, 1973; Bishop, 1973) was motivated by a search for the ^{6}Li analog (at about 15.2 MeV) of an 11.5 MeV 0^+ state

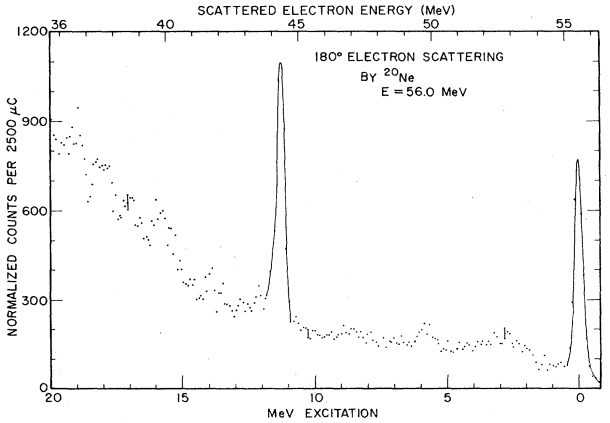

FIG. 18. Spectrum of 56.0 MeV electrons scattered at 180° from ^{20}Ne [figure from Bendel *et al.* (1971)].

[6] See references: Barber *et al.*, 1960; Bernheim and Bishop, 1963; Goldemberg *et al.*, 1964; Hutcheon *et al.*, 1968; Hutcheon and Caplan, 1969; Neuhausen and Hutcheon, 1971.

[7] See references: Kossanyi-Demay, 1966; Spamer and Gudden, 1965; Spamer, 1966.

[8] See references: Barber and Gudden, 1959; Barber *et al.*, 1960; Dudelzak and Taylor, 1961; Edge and Peterson, 1962; Goldemberg *et al.*, 1964; Gudden, 1964; Proca, 1966; Peterson, 1967; Donnelly *et al.*, 1968; Vanpraet and Kossanyi-Demay, 1969; deVries, 1972; Spamer *et al.*, 1972; Chertok *et al.*, 1973.

[9] See references: Edge and Peterson, 1962; Barber *et al.*, 1963; Kossanyi-Demay and Vanpraet, 1966; Clerc and Kuphal, 1968.

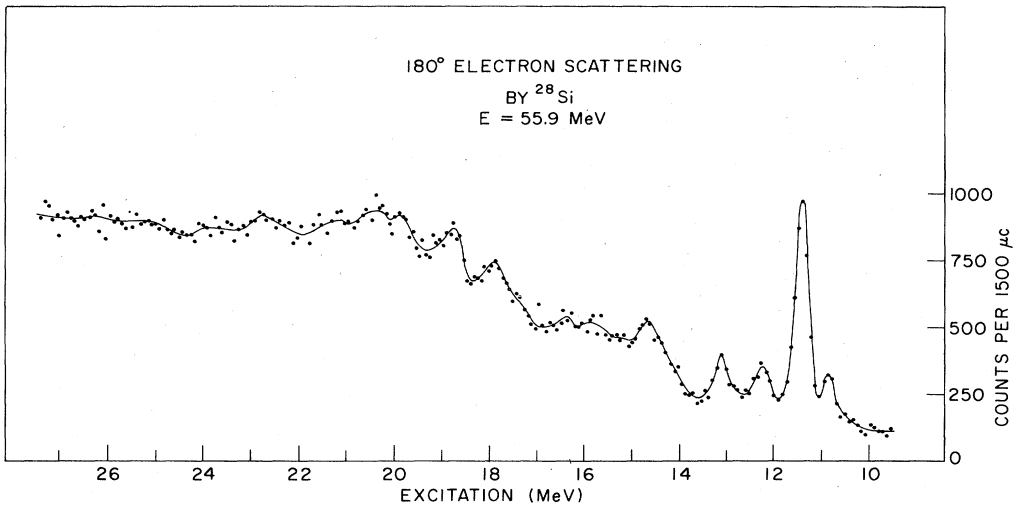

FIG. 19. Spectrum of 55.9 MeV electrons scattered at 180° from ^{28}Si. The 11.41 MeV peak is comparable in height to the elastic peak, not shown [figure from Fagg *et al.* (1969)].

in ^{6}Be proposed (Fowler, 1972; Fetisov and Kopysov, 1972) to explain the low flux of high energy solar neutrinos (Davis *et al.*, 1971; Trimble and Reines, 1973). All three experiments found a negative result, e.g., in Fig. 16 a flat spectrum was observed from 8 to 18 MeV excitation [$\Gamma_0 < 3$ eV, upper limit at 15 MeV (Fagg *et al.*, 1973)].

Another example is the 15.11 MeV transition in ^{12}C where an accurate measurement (Chertok *et al.*, 1973) of Γ_0 had as an additional reason the exploitation of the physical unity of weak and electromagnetic processes found in the $A = 12$ system (O'Connell *et al.*, 1972) by using the measurement of Γ_0 to increase the exactness of the weak magnetism test in β decay and μ capture. Also, in ^{12}C a measurement (Cecil *et al.*, 1974) of Γ_0 for the $\Delta T = 0$, M1 transition at 12.71 MeV (note the intensity comparison with the 15.11 MeV, $\Delta T = 1$ transition in Fig. 17) resulted in a model-dependent measurement of the isospin mixing between the $\Delta T = 0$ and 1 levels.

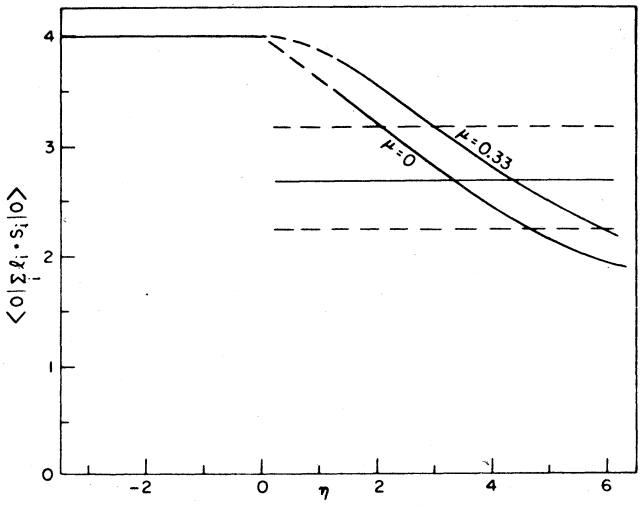

FIG. 20. Curves of $\langle \Sigma l \cdot s \rangle$ vs. η, the deformation parameter in the Nilsson model, for two values μ, the coefficient of the l^2 term in the Nilsson Hamiltonian. The experimental value of the M1 transition strength sum from the 11.24 MeV transition alone is given by the horizontal solid line with the error limits given by the dashed lines [figure from Bendel *et al.* (1971)].

A fourth example is the study of the weak 2.313 MeV transition in ^{14}N (Ensslin *et al.*, 1974) motivated by the fact that an accidental cancellation occurring in the β-decay matrix element of the ^{14}C decay imposes a strong constraint on the range of valid ^{14}C and ^{14}N ground state wavefunctions, making it possible to test models of the nuclear force. A review (Rose *et al.*, 1968) of the β- and γ-decay data on mass 14 concluded that the smallness of the $^{14}\text{C} \rightarrow {}^{14}\text{N}$ β-decay matrix element is due to the presence of a tensor force.

In the *s–d* shell M1 strength concentration supporting Kurath's theory is found in the transitions at 11.24 MeV in ^{20}Ne (Bendel *et al.*, 1971), at 9.96 and 10.72 MeV in ^{24}Mg (Titze and Spamer, 1966; Fagg *et al.*, 1968; Titze, 1969; Fagg *et al.*, 1970a; Johnston and Drake, 1974), and at 11.41 MeV in ^{28}Si (Edge and Peterson, 1962; Goldemberg *et al.*, 1964; Liesem, 1966; Drake *et al.*, 1968; Fagg *et al.*, 1969). The spectra of ^{20}Ne and ^{28}Si shown in Figs. 18 and 19 respectively, demonstrate this concentration, where in each case the dominant inelastic peak is comparable in height to the elastic (not shown in Fig. 19).

Shell model calculations (Maripuu and Wildenthal, 1972) show that the 11.24 MeV transition in ^{20}Ne which contains all of the observed M1 strength in Fig. 18 proceeds primarily by orbital recoupling and not by the spin-flip mechanism. The competition between these mechanisms will be briefly discussed below in Sec. B2. Also in ^{20}Ne a comparison of the experimental result with the curve of $\langle \sum l \cdot s \rangle$ vs η based on the Nilsson model has been made as shown in Fig. 20 where curves are given for two values of the parameter μ, the coefficient of the orbit–orbit $\mathbf{l}^2$ term in the Nilsson Hamiltonian. Inspection of the figure shows that this nucleus is no more prolate than is indicated by a value of $\eta = 4$, in approximate agreement with that of 4.5 calculated by Drake and Singhal (1972). This is an example of how

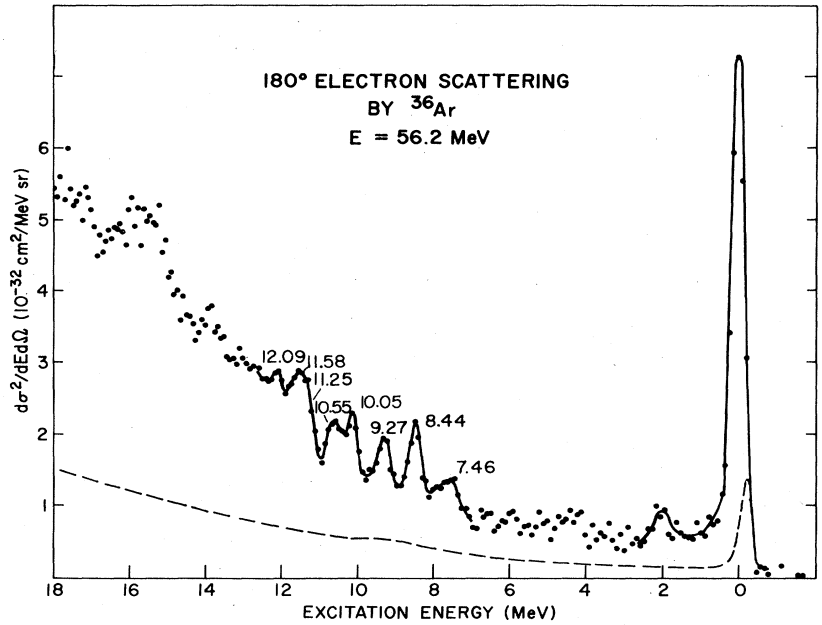

FIG. 21. Spectrum of 56.2 MeV electrons scattered at 180° from ^{36}Ar. If the ordinate is regarded as arbitrary counting rate, the dashed curve gives a comparison of the counting rate resulting from the two Havar foils [target chamber (Fagg *et al.*, 1970) evacuated] with that resulting from the chamber-filled condition; it is not a cross-section curve [figure from Fagg *et al.* (1972)].

the sum rule can place some restriction on ground state shapes and wave functions.

For ^{28}Si in Fig. 19 there is M1 strength primarily at 11.41 MeV along with the two "satellite" transitions at 10.86 and 12.27 MeV. M2 strength resides in the 13–14 MeV region while the peaks beyond 15 MeV are probably due to E1 transitions which have been observed at more forward angles (Gulkarov *et al.*, 1968). An identical pattern prevails in ^{24}Mg where M1 transitions are found around 10 MeV, M2 transitions around 13 MeV, and electric transitions, observed also in forward angle studies (Titze *et al.*, 1967), at higher excitation. These qualitative results for the electric transitions support the statements in Sec. II.A concerning the enhanced ability at 180° to excite electric transitions at higher excitation energies. In fact it has been pointed out (Belyi and Kabachnik, 1972) that transverse form factors are considerably more sensitive than longitudinal ones to the configuration composition of the level wave functions in the giant resonance region.

The ^{28}Si $(t, {}^3\mathrm{He})^{28}$Al reaction (Flynn *et al.*, 1974) was used to study in ^{28}Al the charge exchange mode of the M1 transitions in ^{28}Si. It is of interest to note that in ^{28}Al the intensities of the four transitions of lowest excitation energy follow approximately the same pattern as in the four of lowest energy electroexcited in ^{28}Si (Fagg *et al.*, 1969).

After early work on ^{32}S (Barber *et al.*, 1963; Kossanyi-Demay and Vanpraet, 1966), considerable fragmentation of M1 strength was later found in this nucleus (Fagg *et al.*, 1971) as well as in ^{36}Ar (Fagg *et al.*, 1972), which is apparent in Fig. 21. Note that not all of the peaks in this figure correspond to M1 transitions. Using an adiabatic model of a triaxially deformed rotor, Kurath (1972) showed that more fragmentation would occur in ^{32}S than for an axially symmetric model and stated that the inclusion of Coriolis coupling might induce further fragmentation.

The NRL results of M1 transition strength measurements for all of the self-conjugate *s–d* shell nuclei are summarized in Fig. 22 where each measurement is normalized to the maximum possible total M1 strength expected using Kurath's sum rule, i.e., corresponding to a spherical nucleus in the independent particle shell model. The increase in fragmentation in passing from ^{28}Si to ^{32}S is not as apparent here as it is visually in the spectra, but is nevertheless present. A summary of the *p*-shell self-conjugate nuclei is included with the other *p*-shell nuclei in Fig. 27 discussed below in Section B2.

The Kurath rule predicts essentially no M1 strength in ^{16}O or ^{40}Ca. However, it should be noted that M1 transi-

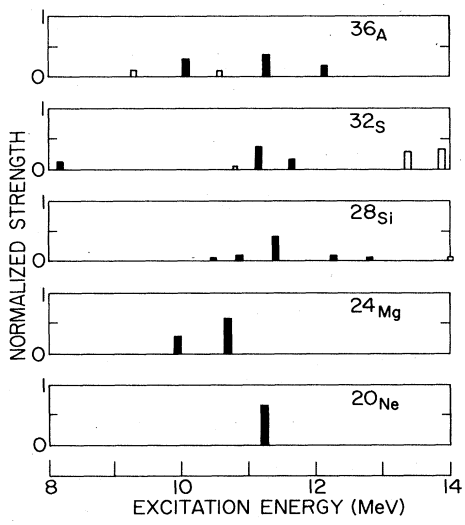

FIG. 22. Strength of M1 transition vs. excitation energy for self-conjugate nuclei of the *s–d* shell. The strengths are normalized to the total M1 strength expected using Kurath's sum rule for a spherical nucleus in the independent particle shell model [figure from Fagg (1973)].

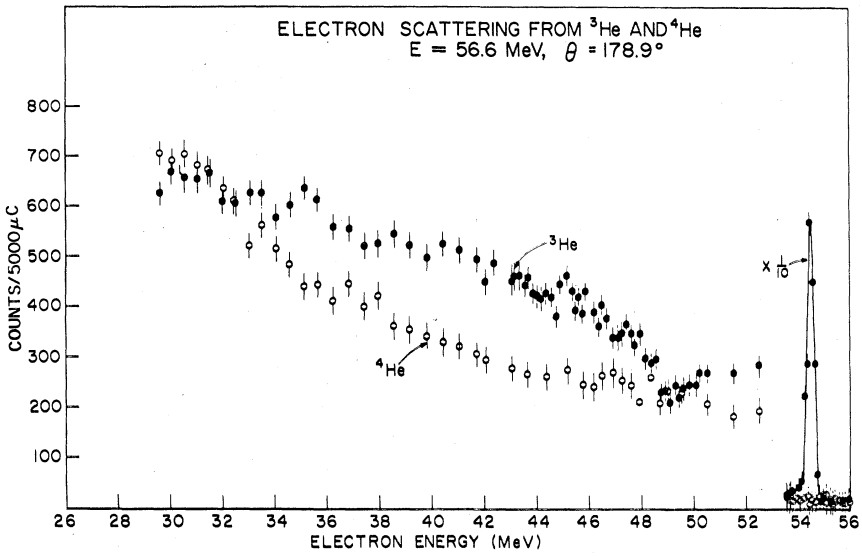

FIG. 23. Normalized spectra of 56.6 MeV electrons scattered at 180° from ^{3}He and ^{4}He (here the average scattering angle of 178.9° is given). The filled circles correspond to ^{3}He and the unfilled circles to ^{4}He [figure from Chertok *et al.* (1969)].

tions have been observed at 16.21 and 10.34 MeV in ^{16}O (Stroetzel and Goldmann, 1970) and ^{40}Ca (Fagg *et al.*, 1971), respectively. The existence of the 10.34 MeV M1 transition is given some support by reports of a 1^+ level in ^{40}K (Twin *et al.*, 1970; Wechsung *et al.*, 1971; James *et al.*, 1971) at 2.290 MeV, which may be the analog of the ^{40}Ca level. Transitions not mentioned in the text above are, however, included in the summary of results presented in Table II.

B. Non-self-conjugate nuclei

1. Preliminary remarks

In these nuclei it is important to understand how the M1 strength becomes fragmented with the addition of one to three nucleons (or holes) to a self-conjugate nucleus. It is also of interest to see how 180° electron scattering can highlight some of the collective rotational features in odd-A nuclei and contribute to their understanding.

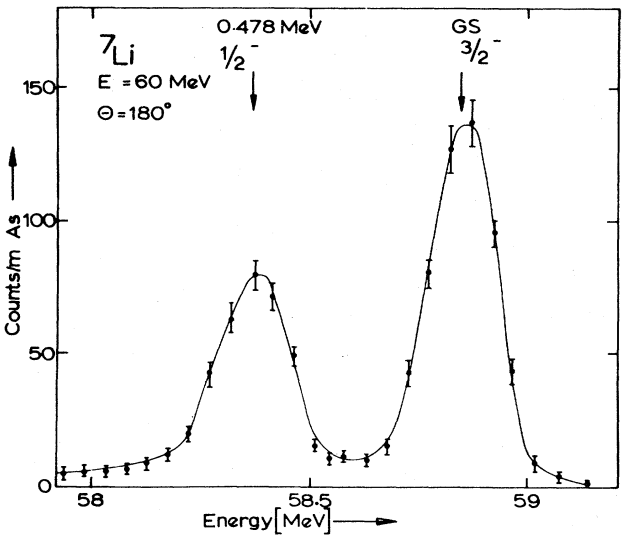

FIG. 24. Spectrum of 60 MeV electrons scattered from ^{7}Li using the IKO Amsterdam 180° scattering system. The separation of the elastic peak and the 0.478 MeV inelastic peak is apparent [figure from Van Niftrik *et al.* (1971a)].

However, perhaps of most recent importance is the study of giant magnetic dipole resonances in heavy nuclei near or at closed shells. If one accepts for a qualitative definition of a giant resonance, one in which a majority of the transition strength resides in a relatively small excitation energy region, then some of the resonances in these nuclei appear to qualify.

2. $A < 40$ nuclei

The examination of ^{3}He using 180° electron scattering, the product of a joint American University–NRL effort (Chertok *et al.*, 1969), was the first study of the M1 continuum in this nucleus. The experiment was primarily a difference measurement between ^{3}He and ^{4}He, the normalized spectra for which are shown in Fig. 23. In the elastic region can be seen the striking contrast between the magnetic scattering from ^{3}He and the pure charge scattering from ^{4}He at 180°. Such a phenomenon is only observable in the very light nuclei since the Z^2 charge-scattering dependence soon begins to produce elastic peaks in heavier nuclei due to the effects of finite solid angle and of multiple scattering and straggling in the target. The greater intensity of the ^{3}He continuum in the 0–5 MeV excitation region is due to magnetic bremsstrahlung. At 5.5 MeV and 7.7 MeV excitation are the two- and three-body breakup thresholds, respectively. The continuum strength in ^{3}He can be explained since a selection rule which prohibits an M1 transition from the 92% S-state component of the ground state to the continuum is only valid for $q = 0$, and rapidly breaks down as q is increased (O'Connell and Gibson, 1973). The role that meson exchange currents play in the continuum strength is as yet unclear.

In some cases in the p-shell nuclei the addition of nucleons to a self-conjugate core does not cause a large degree of fragmentation. This is apparent in the stronger transitions at 0.478 MeV in ^{7}Li (Van Niftrik *et al.*, 1971; Lapikas, 1970), at 3.69 and 15.11 MeV in ^{13}C (Peterson,

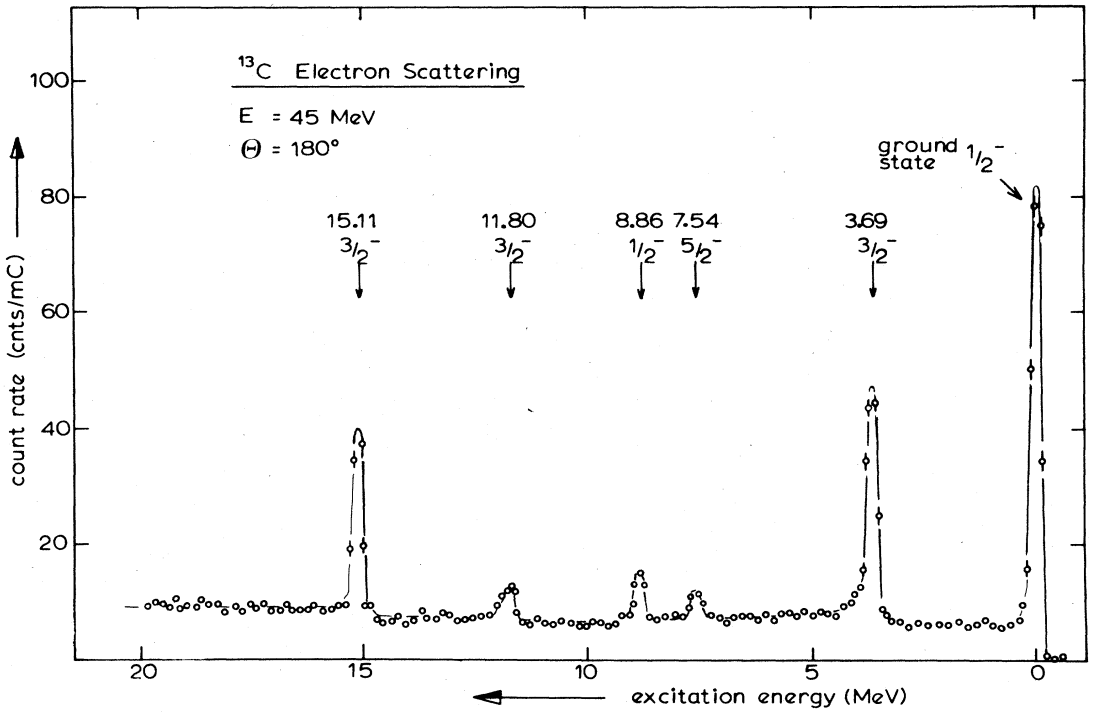

FIG. 25. Spectrum of 45 MeV electrons scattered from ^{13}C using the 180° scattering system at IKO Amsterdam [figure from Lapikas *et al.* (1974)].

1967; Wittwer *et al.*, 1970; Lapikas *et al.*, 1974), at 11.3 MeV in ^{14}C (Crannell *et al.*, 1973), and at 6.32 MeV in ^{15}N (Beer *et al.*, 1968), respectively. The spectra showing these effects in ^{7}Li and ^{13}C are presented in Figs. 24 and 25 which exhibit the fine resolution of the Amsterdam system. The dominance of the 11.3 MeV peak in the spectrum from a radioactive target of ^{14}C is evident in Fig. 26.

On the other hand more fragmentation appears in ^{9}Be and ^{11}B. In ^{9}Be M1 transitions are observed at 2.44, 3.04, 14.39, 15.97, and 16.96 MeV (Barber *et al.*, 1960; Edge and Peterson, 1962; Clerc *et al.*, 1966; Clerc *et al.*, 1968; Slight *et al.*, 1973; Bergstrom *et al.*, 1973). In ^{11}B such transitions are observed at 2.12, 4.44, 5.02, 8.57, and 8.93 MeV (Edge and Peterson, 1962; Kossanyi-Demay and Vanpraet, 1966; Spamer, 1966; Spamer and Artus, 1967; Kan *et al.*, 1974). Except for ^{14}C, the M1 transition strengths in the *p* shell are summarized (Clerk, 1968) in Fig. 27 (the self-conjugate nuclei are also included) where the relatively small degree of strength fragmentation can be noted in ^{7}Li, ^{13}C, and ^{15}N.

In the *s–d* shell considerable fragmentation of M1 strength occurs in ^{22}Ne and ^{26}Mg when two neutrons are added to a "self-conjugate core." This is apparent in the ^{22}Ne spectrum presented in Fig. 28 (Maruyama *et al.*, 1974). It is important to note that these ^{22}Ne results were compared with shell model calculations (Preedom and Wildenthal, 1972); and the theoretically predicted energy positions of, and relative transition strengths to, 1^+ levels in the excitation region studied ($\omega < 13$ MeV) are in good general agreement with experiment.

Tentative results of a theoretical study of ^{22}Ne (Lindgren, 1974) have shown that the orbital recoupling mechanism which dominates in the 11.24 MeV transition in ^{20}Ne is less prevalent here. Especially the higher excitation transitions in ^{22}Ne tend to be spin-flip transitions. This may be qualitatively understood in view of the larger number of neutrons available for spin-flip transitions and the higher excitation energies being closer to the energy centroid of the $d_{3/2}$ single-particle strength.

In ^{26}Mg (Titze and Spamer, 1966; Bendel *et al.*, 1968; Lees *et al.*, 1974) strength fragmentation occurs into several levels between 8.5 and 13.5 MeV excitation. However, in a grosser sense there is still some concentration, since all this strength resides within an energy range of about 5 MeV.

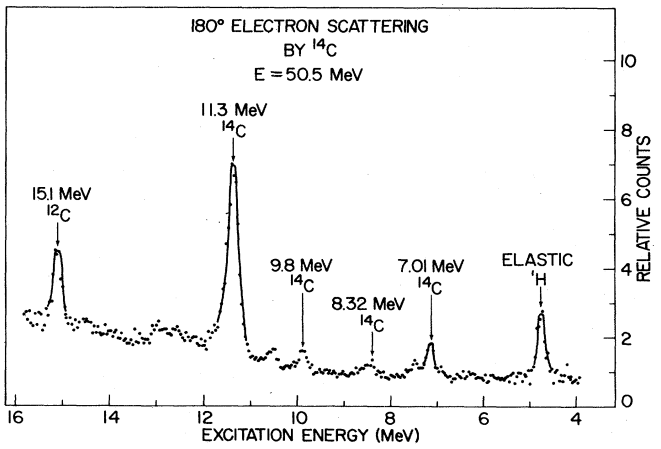

FIG. 26. Spectrum of 50.5 MeV electrons scattered at 180° from ^{14}C. Hydrogen and ^{12}C contamination peaks are at 4.8 and 15.1 MeV, respectively [figure from Crannell *et al.* (1973)].

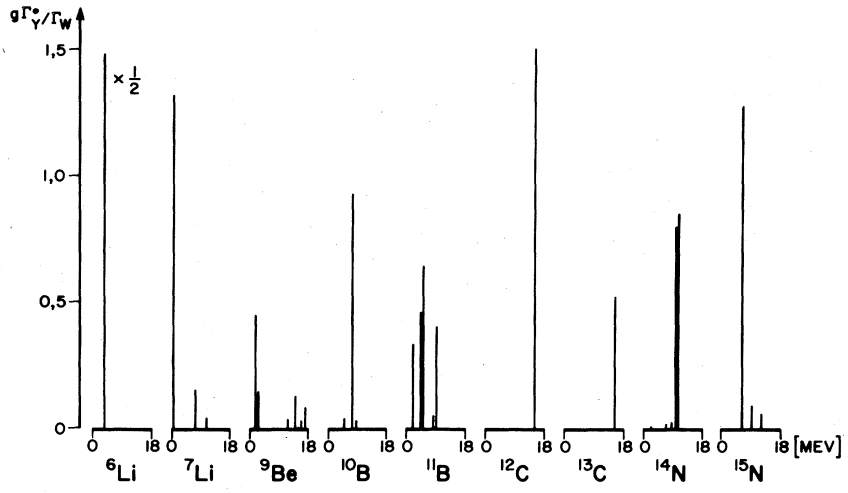

FIG. 27. Strengths of M1 transitions in $1p$ shell nuclei (in Weisskopf units) vs. excitation energy. Most, but not all, transitions shown are from electroexcitation results. $g = (2J + 1)/(2J_0 + 1)$ [figure from Clerc, (1968)].

An interesting example of how 180° electron scattering can highlight the rotational features in an odd-A nucleus is found in ^{25}Mg (Fagg *et al.*, 1969a). The spectrum taken at 180° is shown in Fig. 29. Although many levels exist in the 0–5.8 MeV excitation range that would ordinarily be reached by an M1 transition, only that at 1.60 MeV is excited. This result constitutes a convincing example of the $\Delta K = 0, \pm 1$ selection rule, for the 1.60 MeV level is the $\frac{7}{2}^+$ first excited state of the $K = \frac{5}{2}^+$ ground-state rotational band, while all other candidates in the 0–5.8 MeV region belong to $K = \frac{1}{2}^+$ bands. The peak at 7.81 MeV corresponds to the unresolved $T = \frac{3}{2}$ analogs of the ground, $\frac{5}{2}^+$, and first excited, $\frac{3}{2}^+$, states in ^{25}Na, which are 90 keV apart. In ^{27}Al (Barber *et al.*, 1963; Lombard and Bishop, 1967; 1967a; Bendel *et al.*, 1974) particularly below 2.9 MeV excitation, rotational features similar to those in ^{25}Mg prevail, since the only prominent transition is to the $\frac{7}{2}^+$ state at 2.21 MeV, the first excited state of the $K = \frac{5}{2}^+$ ground state band.

Some study has also been made of ^{23}Na (Barber and Vanpraet, 1965), ^{39}K (Webb *et al.*, 1974), and ^{31}P (Barber *et al.*, 1963; Kossanyi-Demay and Vanpraet, 1966a). Due to disagreement in the ^{31}P observations, they are not included in the summary of results given in Table II.

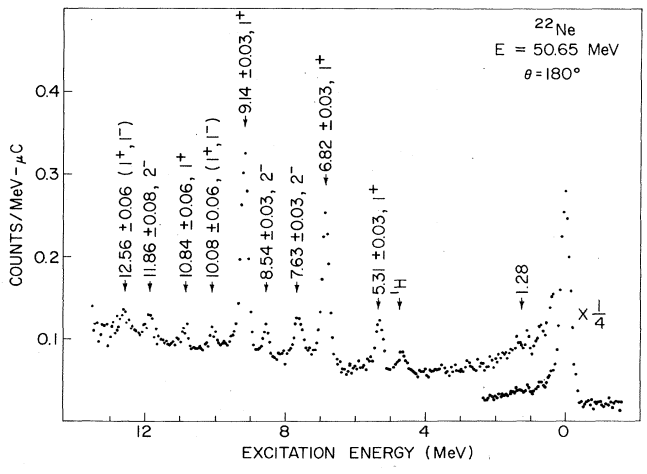

FIG. 28. Spectrum of 50.65 MeV electrons scattered at 180° from ^{22}Ne. The spin assignments determined from the analysis described in the text are given for each of the levels corresponding to the peaks appearing in the spectrum, except that at 1.28 MeV [figure from Maruyama *et al.* (1974)].

3. $A > 40$ nuclei

In the fp shell, work done on ^{55}Mn (Theissen *et al.*, 1969) reveals evidence for some M1 strength in the 1.88 and 2.29 MeV transitions. As the first step in a systematic program to study the relative contributions of M1 strength to the $T_>$ and $T_<$ states among the isotopes of nickel, an NRL–NBS collaborative group (Lindgren *et al.*, 1974) has studied ^{58}Ni and ^{60}Ni. The ^{58}Ni spectra show structure in regions centered at 6.5, 8.5, and 10.5 MeV. The two lower energy regions are, at least in part, tentatively associated with M2 transitions to $T = 1$ states. Peaks at 10.15, 10.55, 10.65, and 11.05 MeV in ^{58}Ni result from M1 transitions to $T = 2$ states. This is probably also true of a peak at 9.81 MeV. Just as in ^{28}Si and ^{28}Al (see Sec. A.3), charge exchange M1 transitions have been observed to analogs of these states in ^{58}Co (Flynn and Garrett, 1972) using the $(t, {}^3\text{He})$ reaction.

A joint SUNY–NRL investigation (Cecil *et al.*, 1973; Fagg *et al.*, 1973a) was made to observe M1 strength produced by spin-flip transitions from the filled $g_{9/2}$ neutron shell in ^{90}Zr. Although structure from 7.5 to 10.5 MeV, peaking at about 9 MeV, was observed in the spectrum at $E = 60$ MeV, no structure was evident at $E = 37$ MeV. Thus, the amount of M1 strength present is unclear.

Using natural targets of La, Ce, and Pr the Darmstadt group (Pitthan and Walcher, 1971; Pitthan and Walcher, 1972; Pitthan, 1973) observed an enhancement of the intensity of a broad peak at about 9 MeV in their spectra at backward angles. This is apparent in the spectra of Ce shown in Fig. 30. This is evidence for a general M1 resonance among these nuclei at that excitation energy and was the first electron scattering evidence for such a resonance in the heavy nuclei. In Fig. 31 the broad peak (~3 MeV FWHM) at 7.9 MeV observed (Lone *et al.*, 1974) in a 180° scattering study of ^{197}Au is most consistent with the assumption of a group of M1 transitions in this excitation region. Spin-flip transitions primarily from the $h_{11/2}$ proton and $i_{13/2}$ neutron shells may be responsible for much of this strength.

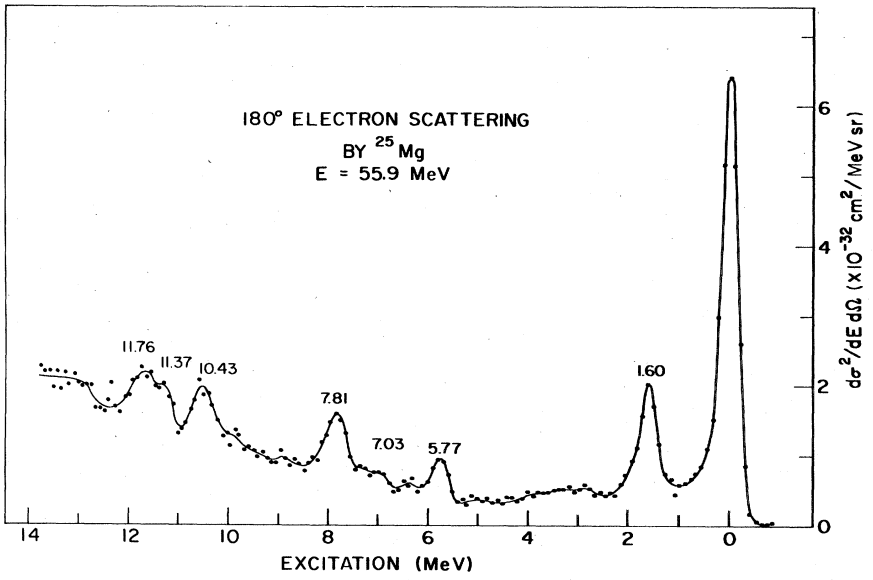

FIG. 29. Spectrum of 55.9 MeV electrons scattered at 180° from ^{25}Mg [figure from Fagg *et al.* (1969a)].

The possibility for such spin-flip transitions is even greater for the lead isotopes. Still in progress is a study of ^{206}Pb using 180° scattering (Lone *et al.*, 1974a) which reveals peaks at 6.1, 6.9, 7.3, and 7.95 MeV. This structure is remarkably similar to that in ^{208}Pb where more forward angle (Walcher, 1973) and 180° (Ensslin *et al.*, 1973;

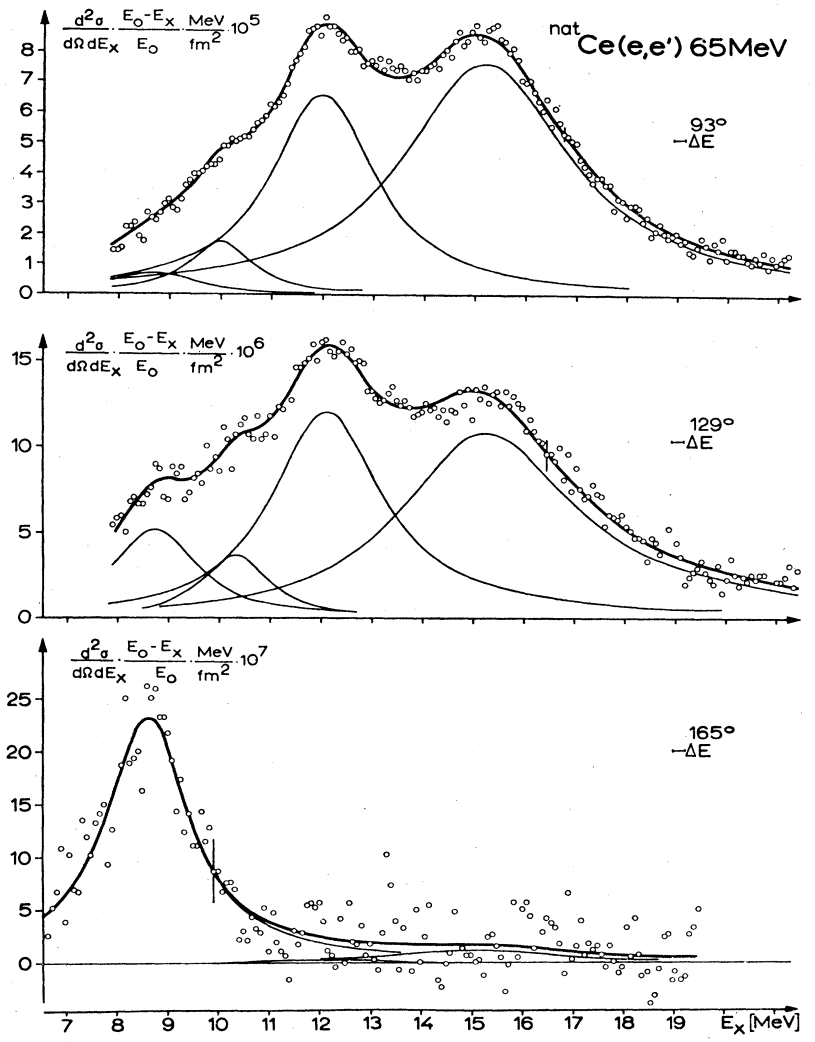

FIG. 30. Spectra of 65 MeV electrons scattered at three different angles from ^{nat}Ce. At 165° the increased intensity of the structure at 9 MeV is apparent [figure from Pitthan (1973)].

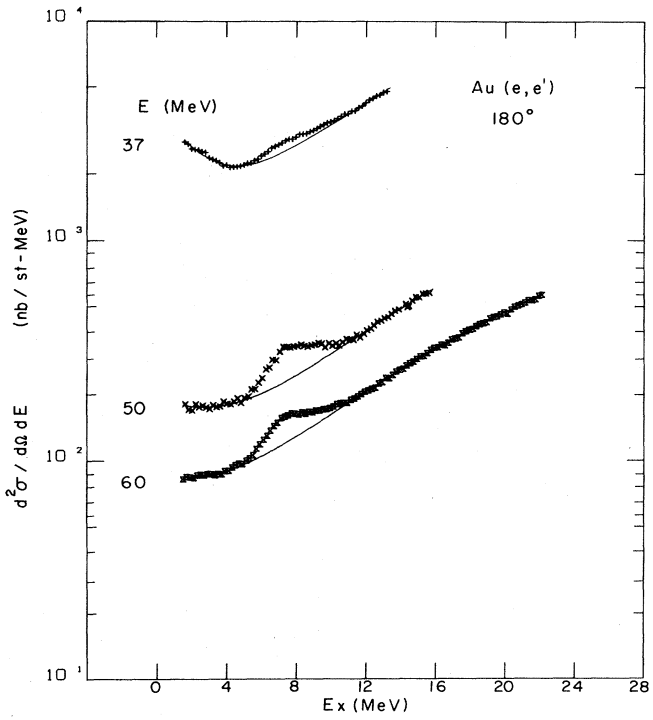

FIG. 31. Spectra of 37, 50, and 60 MeV electrons scattered at 180° from ^{197}Au [figure from Lone *et al.* (1974)].

Bendel *et al.*, 1973; Fagg *et al.*, 1973a) scattering observations reveal peaks at 6.2, 7.3, and 7.9 MeV, e.g., as seen in Fig. 32.[10] The structure at 7.3 MeV appears to be an unresolved group of transitions whose average intensity increases with increasing q somewhat more rapidly than the peaks at 6.2 and 7.9 MeV. The peak at 7.9 MeV may be associated with the M1 structure observed at this excitation by threshold photoneutron techniques (Bowman *et al.*, 1970; Toohey and Jackson, 1972).[11] M1 transition strength at about this excitation energy is predicted theoretically

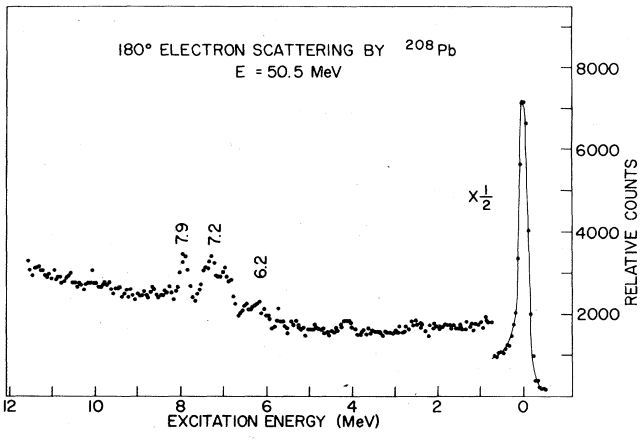

FIG. 32. Spectrum of 50.5 MeV electrons scattered at 180° from ^{208}Pb [figure from Bendel *et al.* (1973); Fagg *et al.* (1973a)].

[10] The inference in Fagg *et al.* (1973a) that the 6.2 and 7.9 MeV transitions are known M1 transitions is erroneous.

[11] However, see Harvey *et al.* (1973).

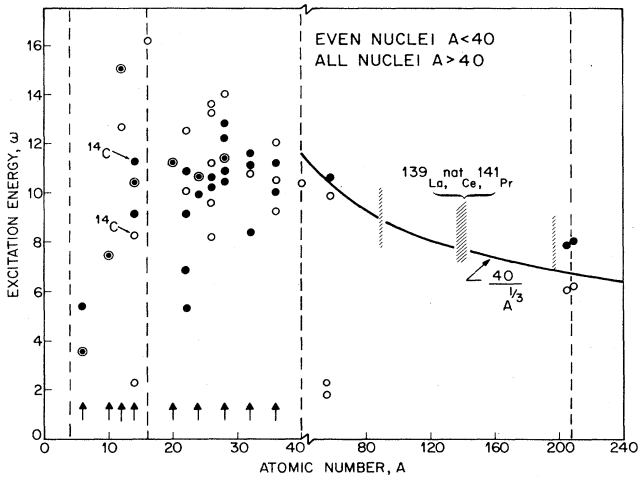

FIG. 33. Plot of excitation energies of M1 transitions vs. atomic number. In order to present better the trends involved, only the transitions in even nuclei are plotted for $A < 40$. For $A > 40$ all are plotted and are compared with $\omega = 40/A^{\frac{1}{3}}$ (Hanna, 1974). Dashed lines indicate locations of doubly closed shells. Arrows indicate self-conjugate nuclei. Open circles represent uncertain transitions. Encircled black points represent the strongest transition in each self-conjugate nucleus of $A \leq 28$. Hashed areas indicate broad peaks or regions of unresolved structure. Note change in horizontal scale at $A = 40$. *Note added in proof:* Several transitions in ^{58}Ni and ^{60}Ni ($\omega \sim 11$ MeV) have not been included. Also, the closed circles at about 8 MeV in ^{206}Pb and ^{208}Pb should be open.

(Vergados, 1971; Ring and Speth, 1973). The situation in ^{208}Pb needs much clarification.

Although much work in this region of the nuclides remains to be done, the pattern that seems to be emerging is one which exhibits considerable M1 transition strength in the 7 to 9 MeV excitation region. It should also be noted that with (γ, γ') experiments (Wolf *et al.*, 1972), M1 strength in this excitation region has been observed in ^{141}Pr, ^{144}Nd, ^{205}Tl, ^{208}Pb, and ^{209}Bi. Evidence for an M1 giant resonance comparable in universality to the well-known E1 resonance seems to be growing. In this connection Fig. 33 gives a plot of the excitation energy ω for most of the known electroexcited M1 transitions as a function of A. The data for $A > 40$ are compared with a curve given by $\omega = 40/A^{\frac{1}{3}}$ (Hanna, 1974).

In the foregoing discussion of experimental results it has only been possible to make selected comments based on the author's judgement; much worthy work has not been adequately discussed. However, an attempt at a complete summary of results is presented in Table II.

V. TABLE OF RESULTS AND GLOSSARY OF SYMBOLS

The following table summarizes the results of measurements on the electroexcitation of M1 transitions known to the author up to December, 1974. While completeness has been attempted, no claim of it is made. When known, electroexcited E2 components have also been included (denoted by [E2] after the entry) as well as the maximum scattering angle, θ_{max}, of the experiment, and the isospin quantum number, T, of the level excited. These three entries are somewhat more susceptible to lack of completeness than the others. When available, transition

TABLE II. Ground-state transition widths of electroexcited M1 transitions and spin assignments of states excited.

Nucleus, J_0^π, T_0	Excitation energy, ω (MeV)	J^π, T	Γ_0 (eV)	Γ_0/Γ_W	R_{tr} (fm)	θ_{max} (degrees)	Reference
^{6}Li, 1^+, 0	3.56	0^+, 1				160	Barber *et al.*, 1960
						180	Barber *et al.*, 1963
						120	Bernheim and Bishop, 1963; Bernheim, 1965
						180	Goldemberg *et al.*, 1964
						155	Hutcheon *et al.*, 1968; Hutcheon and Caplan, 1969
			8.36 ± 0.36	8.8	2.80 ± 0.10	153	Eigenbrod, 1969
	5.36	2^+, (1)	$\begin{pmatrix}0.19\pm0.04\\0.08\pm0.04\end{pmatrix}$	$\begin{pmatrix}0.059\\0.025\end{pmatrix}$		155	Hutcheon *et al.*, 1970
						80	Neuhausen and Hutcheon, 1971
^{7}Li, $\frac{3}{2}^-$, $\frac{1}{2}$	0.478	$\frac{1}{2}^-$, $\frac{1}{2}$	$((2.74\pm0.40)10^{-7})$[E2]	17		120	Bernheim and Bishop, 1963, 1963a; Bernheim, 1965
						162	Chertok and Booth, 1965
			$(6.30\pm0.31)10^{-3}$	2.8	2.88 ± 0.07	180	Van Niftrik *et al.*, 1971
			$((2.8\pm1.6)10^{-7})$[E2]	17			
	11.28	$\frac{3}{2}^-$,	1.3 ± 0.4^{ba}	0.043		153	Artus *et al.*, 1967
^{9}Be $\frac{3}{2}^-$, $\frac{1}{2}$	2.44	$\frac{5}{2}^-$,				160	Barber *et al.*, 1960
						180	Edge and Peterson, 1962
			$(8.9\pm1.0)10^{-2}$	0.30	2.7 ± 0.5	165	Clerc *et al.*, 1968
			$(1.89\pm0.13)10^{-3}$[E2]	23.8			
	3.04	$\frac{1}{2}^-$,	0.18 ± 0.09	0.30	2.9 ± 0.9		
	14.39	$\frac{3}{2}^-$, $\frac{3}{2}$				180	Edge, 1962
			8.1 ± 0.8	0.13	1.9 ± 0.6	165	Clerc *et al.*, 1968
			6.2 ± 0.6	0.10		153	Bergstrom *et al.*, 1973
	15.97	$(\frac{3}{2})^-$,	2.6 ± 0.7	0.030		165	Clerc *et al.*, 1968
	16.63	$(\leq\frac{5}{2}^-)$,	$((2.0\pm0.5)g)$	$(0.021g)$		153	Bergstrom *et al.*, 1973
	16.97	$\frac{1}{2}^-$, $\frac{3}{2}$	8.6 ± 0.9	0.084	2.1 ± 0.6	165	Clerc *et al.*, 1968
			11.5 ± 1.4	0.11		153	Bergstrom *et al.*, 1973
	17.28	$(\leq\frac{5}{2}^-)$,	$((7.3\pm1.3)g)$	$(0.065g)$			
^{10}B, 3^+, 0	7.48	$2,^+1$				180	Kossanyi-Demay and Vanpraet, 1966
			12.0 ± 2.2^{ba}	1.4	2.70 ± 0.20^{ba}	165	Spamer, 1966
^{11}B, $\frac{3}{2}^-$ $\frac{1}{2}$	2.12	$\frac{1}{2}$, $-\frac{1}{2}$				180	Edge and Peterson, 1962
						165	Spamer, 1966
			0.16 ± 0.016^{ba}	0.79		180	Kossanyi-Demay and Vanpraet, 1966
			0.14 ± 0.04	0.70		145	Kan *et al.*, 1974
	4.44	$\frac{5}{2}^-$, $\frac{1}{2}$				180	Edge and Peterson, 1962
						180	Kossanyi-Demay and Vanpraet, 1966
			0.60 ± 0.09	0.32	2.60 ± 0.35^{ba}	165	Spamer and Artus, 1967
			$(16.4\pm2.1)10^{-3}$[E2]	7.9	3.44 ± 0.50^{ba}		
			0.73 ± 0.07	0.39		145	Kan *et al.*, 1974
			$(2.0\pm0.2)10^{-2}$[E2]	9.7			
	5.02	$\frac{3}{2}^-$, $\frac{1}{2}$				180	Edge and Peterson, 1962
						180	Kossanyi-Demay and Vanpraet, 1966
			1.73 ± 0.14	0.65	2.60 ± 0.15^{ba}	165	Spamer and Artus, 1967
			2.12 ± 0.21	0.80		145	Kan *et al.*, 1974
	8.57	$\frac{3}{2}^-$, $\frac{1}{2}$	0.72 ± 0.30^{ba}	0.055		165	Spamer, 1966
			$0.40\pm.1$[E2]^{ba}	7.3	3.90 ± 0.50^{ba}		
			0.73 ± 0.07	0.06		145	Kan *et al.*, 1974
			0.23 ± 0.03[E2]	4.2			
	8.93	$\frac{5}{2}^-$, $\frac{1}{2}$				180	Kossanyi-Demay and Vanpraet, 1966
			4.0 ± 0.6^{ba}	0.27	2.65 ± 0.21^{ba}	165	Spamer, 1966
			4.93 ± 0.50	0.33		145	Kan *et al.*, 1974
	13.0	$(\frac{1}{2}^-)$, $(\frac{3}{2})$	(36 ± 7)	(0.78)			
			(2.2 ± 0.2)[E2]	(5.0)			
		$(\frac{3}{2}^-)$, $(\frac{3}{2})$	(18 ± 4)	(0.39)			
			(1.1 ± 0.1)[E2]	(2.5)			
^{12}C, 0^+, 0	12.7	1^+, 0				165	Spamer, 1973
			0.35 ± 0.05	0.008		180	Cecil *et al.*, 1974
	15.11	1^+, 1				160	Barber and Gudden, 1959; Barber *et al.*, 1960
						135	Dudelzak and Taylor, 1961
						180	Edge and Peterson, 1962
						180	Goldemberg *et al.*, 1964

TABLE II. (*Continued*)

Nucleus, J_0^π, T_0	Excitation energy, ω (MeV)	J^π, T	Γ_0 (eV)	Γ_0/Γ_W	R_{tr} (fm)	θ_{max} (degrees)	Reference
			34.4±3.4	0.47		165	Gudden, 1964
						180	Proca, 1966; Proca and Isabelle, 1968
			36±3	0.50		150	Peterson, 1967
			39.5±4[ba]	0.55	2.70±0.20[ba]	180	Vanpraet and Kossanyi-Demay, 1969
			35.74±0.86	0.49			Spamer *et al.*, 1972
			37.0±1.1	0.51		162	Chertok *et al.*, 1973
^{13}C, $\frac{1}{2}^-$, $\frac{1}{2}$	3.69	$\frac{3}{2}^-$,	0.358±0.047	0.34	2.76±0.16	165	Wittwer *et al.*, 1970
			$(3.61\pm0.40)10^{-3}$[E2]	3.52	3.50±0.37		
	8.86	$\frac{1}{2}^-$,	3.36±0.47	0.23	2.50±0.19		
						180	Lapikas *et al.*, 1974
	9.90	$\frac{3}{2}^-$,	0.324±0.049	0.016	2.83±0.25	165	Wittwer *et al.*, 1970
			$(6.3\pm2.1)10^{-3}$[E2]	0.045			
						180	Lapikas *et al.*, 1974
	11.07	$(\frac{1}{2}^-)$,	1.02±0.19	0.036	3.03±0.22	165	Wittwer *et al.*, 1970
		$(\frac{3}{2}^-)$,	0.172±0.057	0.006			
			0.256±0.028[E2]	1.03	4.01±0.27		
						180	Lapikas *et al.*, 1974
	11.80	$\frac{3}{2}^-$,	3.45±0.86	0.10		165	Wittwer *et al.*, 1970
						180	Lapikas *et al.*, 1974
	15.11	$\frac{3}{2}^-$, $\frac{3}{2}$	25±7	0.35		150	Peterson, 1967
			22.7±2.7	0.31	2.55±0.20	165	Wittwer *et al.*, 1970
						180	Lapikas *et al.* 1974
^{14}C, 0^+, 1	7.01	2^+				180	Crannell *et al.*, 1973
	8.32	$(1, 2)^+$,					
	9.8						
	11.3	(1^+),					
^{14}N, 1^+, 0	2.312	0^+, 1				120	Bishop *et al.*, 1964
						120	Bernheim, 1965
			$(1.7\pm0.5)10^{-2}$	0.066		163	Ensslin *et al.*, 1974
	9.17	2^+, 1				180	Edge and Peterson, 1962
						180	Barber *et al.*, 1963
						180	Kossanyi-Demay and Vanpraet, 1966
			7.7±0.9	0.48	2.92±0.23	165	Clerc and Kuphal, 1968
	10.43	2^+, 1				180	Edge and Peterson, 1962
						180	Barber *et al.*, 1963
							Kossanyi-Demay and Vanpraet, 1966
			12.1±1.5	0.51			Clerc and Kuphal, 1968
^{15}N, $\frac{1}{2}^-$, $\frac{1}{2}$	6.32	$\frac{3}{2}^-$,	3.4±0.7	0.64		165	Beer *et al.*, 1968
			$(6\pm2)10^{-2}$[E2]	3.1			
	9.16	$\frac{3}{2}^{(-)}$,	0.75±0.45	0.046		165	Clerc, 1968
			0.10±0.05[E2]	0.85			
	11.88	$\frac{3}{2}^-$,	1.1±0.7	0.030			
			0.48±0.22[E2]	1.1			
^{16}O, 0^+, 0	16.21	1^+,	5.1±0.8	0.05	3.2±0.3	165	Stroetzel and Goldmann, 1970
^{19}F, $\frac{1}{2}^+$, $\frac{1}{2}$	7.7	$\frac{3}{2}^+$,				180	Barber *et al.*, 1963
^{20}Ne, 0^+, 0	11.24	1^+, 1	$11.2_{-1.8}{}^{+2.1}$	0.38	2.53±0.15	180	Bendel *et al.*, 1971
	11.58	(1^+)	0.65±0.18	0.020			
		(2^+),	0.40±0.13[E2]	0.75			
^{22}Ne, 0^+, 1	5.31	1^+, 1	0.127±0.22	0.04	$2.51_{-0.31}{}^{+0.18}$	180	Maruyama *et al.*, 1974
	6.82	1^+, 1	0.611±0.096	0.092	$2.24_{-0.42}{}^{+0.24}$		
	9.14	1^+, 1	2.83±0.26	0.176	$2.85_{-0.14}{}^{+0.11}$		
	10.08	(1^+), 1	(1.13±0.14)	(0.042)	$3.15\pm_{-0.19}{}^{+0.15}$		
	10.84	1^+, 1	$0.66_{-0.17}{}^{+0.14}$	0.025	$2.86\pm_{-0.30}{}^{+0.25}$		
	12.56	(1^+), 1	$(1.34_{-0.65}{}^{+0.86})$	(0.032)	$3.14_{-0.66}{}^{+0.32}$		
^{23}Na, $\frac{3}{2}^+$, $\frac{1}{2}$	4.43	$(\frac{1}{2}^+)$,	0.64±0.06[ba]	0.35		180	Barber and Vanpraet, 1965
^{24}Mg, 0^+, 0	9.85	1^+, 1	1.05±0.26	0.052		153	Titze and Spamer, 1966
	9.97	1^+, 1	4.5. ±0.73	0.22	3.05±0.44		
			$7.6_{-1.4}{}^{+1.6}$	0.36	$2.94_{-0.02}{}^{+0.18}$	180	Fagg *et al.*, 1970
			4.6±0.4	0.22	2.83±0.30	153	Johnston and Drake, 1974
	10.70	1^+, 1	15.9±0.24	0.62	3.22±0.47	153	Titze and Spamer, 1966
			$17.6_{-3.0}{}^{+3.5}$	0.68	$2.94_{-0.15}{}^{+0.13}$	180	Fagg *et al.*, 1970
			13.4±1.2	0.52	2.91±0.04	153	Johnston and Drake, 1974

TABLE II. (*Continued*)

Nucleus, J_0^π, T_0	Excitation energy, ω (MeV)	J^π, T	Γ_0 (eV)	Γ_0/Γ_W	R_{tr} (*fm*)	θ_{max} (degrees)	Reference
^{25}Mg, $\frac{5}{2}^+$, $\frac{1}{2}$	1.60	$\frac{7}{2}^+$, $\frac{1}{2}$	$(4.1_{-0.9}^{+1.1})10^{-2}$	0.48	$2.4_{-0.4}^{+0.3}$	180	Fagg *et al.*, 1969a
	5.77	$(\frac{3}{2}^+)$, $\frac{1}{2}$	$0.92_{-0.35}^{+0.42}$	0.23	$2.0_{-1.5}^{+0.6}$		
	7.03	$(\frac{5}{2}^+)$, $\frac{1}{2}$	$2.2_{-0.8}^{+1.0}$	0.30	3.7 ± 0.5		
	7.81	$\frac{3}{2}^+$, $\frac{5}{2}^+$; $\frac{3}{2}$	$(4.7_{-1.0}^{+1.2})/g$	$0.47/g$	$2.6_{-0.4}^{+0.2}$		
	10.43		$(17\pm5)/g$	$0.72/g$	3.5 ± 0.3		
	11.37		$(12_{-5}^{+6})/g$	$0.4/g$	$3.0_{-0.8}^{+0.6}$		
	11.76		$(18_{-6}^{+7})/g$	$0.5/g$	$3.2_{-0.6}^{+0.4}$		
^{26}Mg, 0^+, 1	8.22	(1^+)				153	Titze and Spamer, 1966
	8.52	(1^+)					
		(1^+)	$0.5_{-0.3}^{+0.4ba}$	0.04	$3.2_{-1.4}^{+0.6ba}$	180	Bendel *et al.*, 1968
		2^+				153	Lees *et al.*, 1974
	9.24	(1^+)				153	Titze and Spamer, 1966
			$3.3_{-0.7}^{+0.9ba}$	0.19	$3.62_{-0.19}^{+0.17ba}$	180	Bendel *et al.*, 1968
	9.29	2^+			3.96 ± 0.44[E2]	153	Lees *et al.*, 1974
	9.67	(1^+)				153	Titze and Spamer, 1966
			$1.7_{-0.6}^{+0.8ba}$	0.091	$2.90_{-0.54}^{+0.36ba}$	180	Bendel *et al.*, 1968
	10.20	1^+				153	Titze and Spamer, 1966
			$5.7_{-1.2}^{+1.3ba}$	0.26	$3.40_{-0.18}^{+0.16ba}$	180	Bendel *et al.*, 1968
			4.8 ± 3.4	0.22	3.32 ± 0.20	153	Lees *et al.*, 1974
	10.65	1^+				153	Titze and Spamer, 1966
			$9.1_{-1.7}^{+2.0ba}$	0.36	3.47 ± 0.14^{ba}	180	Bendel *et al.*, 1968
			6.4	0.25	3.34	153	Lees *et al.*, 1974
	11.20	(1^+)				153	Titze and Spamer, 1966
			$3.9_{-0.1}^{+1.3ba}$	0.13	$3.23_{-0.33}^{+0.26}$	180	Bendel *et al.*, 1968
	13.33	(1^+)				153	Titze and Spamer, 1966
			$14.5_{-3.0}^{+3.3ba}$	0.56	$3.10_{-0.21}^{+0.17ba}$	180	Bendel *et al.*, 1968
	13.66	(1^+)	$2.3_{-1.5}^{+2.4ba}$	0.043	$3.0_{-3.0}^{+0.8ba}$		
^{27}Al, $\frac{5}{2}^+$, $\frac{1}{2}$	2.21	$\frac{7}{2}^+$, $\frac{1}{2}$				135	Lombard and Bishop, 1967; 1967a
						180	Bendel *et al.*, 1974
	2.98	$\frac{3}{2}^+$, $\frac{1}{2}$					
	4.42	$\frac{5}{2}^+$, $\frac{1}{2}$					
	6.50						
	7.57						
	8.05						
	8.74						
	10.68						
	11.69						
	12.30						
^{28}Si, 0^+, 0	10.48	1^+, 1	$2.4_{-0.9}^{+1.2}$	0.099	3.9 ± 0.4	180	Fagg *et al.*, 1969
	10.86	1^+, 1				165	Liesem, 1966
			$5.7_{-1.1}^{+1.3}$	0.21	$2.98_{-0.27}^{+0.23}$	180	Fagg *et al.*, 1969
	11.41	1^+, 1				180	Edge and Peterson, 1962
						180	Goldemberg *et al.*, 1964
			25.7±3.6	0.82	3.0 ± 0.3	165	Liesem, 1966
						155	Drake *et al.*, 1968
			$20.8_{-3.7}^{+4.3}$	0.67	$2.58_{-0.25}^{+0.21}$	180	Fagg *et al.*, 1969
	12.27	1^+, 1				165	Liesem, 1966
			$7.3_{-1.8}^{+2.0}$	0.19	$2.93_{-0.39}^{+0.32}$	180	Fagg *et al.*, 1969
	12.79	1^+, 1	$3.3_{-1.7}^{+2.3}$	0.075	$3.2_{-1.2}^{+0.7}$		
	14.01	$(1^+, 1)$	$(8.9_{-5.0}^{+7.3})$	(0.15)	$(3.8_{-1.1}^{+0.8})$		
^{32}S, 0^+, 0	8.13	1^+, 1	$2.8_{-1.4}^{+1.8}$	0.25	$3.4_{-0.9}^{+0.5}$	180	Fagg *et al.*, 1971
	10.82	$(1^+, 1)$	$(2.9_{-1.4}^{+3.6})$	(0.11)	$(2.0_{-2.0}^{+1.2})$		
	11.14	1^+, 1	$18.9_{-6.3}^{+7.4}$	0.66	3.9 ± 0.3		
	11.62	1^+, 1	$9.7_{-4.8}^{+6.1}$	0.30	$3.4_{-0.9}^{+0.5}$		
^{36}Ar, 0^+, 0	9.27	$(1^+, 1)$	$(1.8_{-0.7}^{+0.9})$	(0.11)	$(2.0_{-2.0}^{+0.8})$	180	Fagg *et al.*, 1972
	10.05	1^+, 1	$6.2_{-1.7}^{+2.0}$	0.29	$3.3_{-0.4}^{+0.3}$		
	10.55	$(1^+, 1)$	$(2.2_{-1.0}^{+1.8})$	(0.09)	$(1.9_{-1.9}^{+1.1})$		
	11.25	1^+, 1	$8.9_{-3.1}^{+3.8}$	0.29	$3.4_{-0.5}^{+0.4}$		
	12.09	$(1^+, 1)$	$(5.0_{-2.6}^{+4.0})$	(0.13)	$(2.3_{-2.3}^{+0.9})$		
^{40}Ca, 0^+, 0	10.34	$(1^+,1)$	$(7.0_{-2.2}^{+2.9})$	(0.30)	$(3.5_{-0.6}^{+0.4})$	180	Fagg *et al.*, 1971
^{55}Mn, $\frac{5}{2}^-$, $\frac{5}{2}$	1.88	$(\frac{7}{2}^-,)$				149	Theissen *et al.*, 1969
			$(0.96\pm0.21)10^{-3}$[E2]	4.0			
	2.29						
^{58}Ni, 0^+, 1	9.81	$(1^+, 2)$	(3.4 ± 0.68)	(0.17)		180	Lindgren *et al.*, 1974
	10.15	1^+, 2	6.5 ± 1.3	0.28			
	10.55	1^+, 2	8.3 ± 1.7	0.33			
	10.65	1^+, 2					
	11.05	1^+, 2	5.3 ± 1.1	0.18			

TABLE II. (*Continued*)

Nucleus, J_0^π, T_0	Excitation energy, ω (MeV)	J^π, T	Γ_0 (eV)	Γ_0/Γ_W	R_{tr} (*fm*)	θ_{max} (degrees)	Reference
^{60}Ni, 0^+, 2	11.89	1^+, 3	8.5±1.7	0.24		180	Lindgren *et al.*, 1974
	12.31	1^+, 3	4.1±0.82	0.10			
	13.12	(1^+, 3)	(≤1.0)	(≤0.021)			
	13.36	(1^+, 3)	(≤1.0)	(≤0.020)			
	13.75	(1^+, 3)	(≤1.0)	(≤0.018)			
^{90}Zr, 0^+, 5	~9					180	Cecil *et al.*, 1973; Fagg, 1973a
^{139}La, $\frac{7}{2}^+$, 25/2	~9					165	Pitthan and Walcher, 1971, 1972; Pitthan, 1973
^{nat}Ce	8.7	(1^+)	(90)	(6)		165	Pitthan and Walcher, 1971 1972; Pitthan, 1973
^{141}Pr, $\frac{5}{2}^+$, 23/2	~9					165	Pitthan and Walcher, 1971, 1972; Pitthan, 1973
^{197}Au, $\frac{3}{2}^+$, 39/2	7.9		(144)	(13.9)		180	Lone *et al.*, 1974
^{206}Pb, 0^+, 21	6.1					180	Lone *et al.*, 1974a
	(6.9)						
	(7.3)						
	7.95						
^{208}Pb, 0^+, 22	6.2					180	Ensslin, 1973, Fagg *et al.*, 1973a, Bendel *et al.*, 1973
	(7.3)						
	7.9						

radii have been included for completeness and for usefulness to experimentalists, despite the doubt as to their physical reality as discussed in Sec. II.B.2. The latest known energy values are given to the nearest 10 keV. The ground-state transition widths are given in both electronvolts and Weisskopf units (i.e., Γ_0/Γ_W). Doubtful values or ambiguous assignments are presented in parenthesis. The ground-state spin, parity, and isospin are given along with each nucleus. When the results given issue from a PWBA analysis with no Coulomb distortion correction, a superscript "*ba*" is added to the value of Γ_0. In instances where the spin of the excited state is uncertain, the Γ_0 are given times the statistical weighting factor $g = (2J_0 + 1)/(2J + 1)$ (or $1/g$).

Continuum transition strengths such as that observed in ^{3}He are not included. Also not included are results which are not substantiated by later work on the same nucleus. In most cases when an author or group follow a work shortly thereafter with more accurate or more complete results, only the later work is cited. When a group of consecutively listed transitions are from a single reference, the reference is given only for the first transition of the group.

GLOSSARY OF SYMBOLS

Some of the symbols listed below may be used at times to denote other quantities in the text. However, when this is the case, such use will be clear from the definitions accompanying them as well as from the context. Other symbols used only rarely are defined in the text.

a	Spin-orbit coupling parameter
A	Atomic number
α	Fine structure constant
$B(XL,q)$	Reduced transition probability where $X = E$ (electric), or M (magnetic)
E, E'	Incident and scattered electron energies, respectively
f_c	Coulomb distortion correction coefficient, $f_c = (d\sigma/d\Omega)_{DWBA}/(d\sigma/d\Omega)_{PWBA}$
Γ_0	Ground-state width for electromagnetic transition to the ground state
H	Nuclear Hamiltonian
J_0, J	Ground and excited state spins, respectively
k	Photon momentum
l	Nuclear orbital angular momentum
L	Transition multipolarity
m	Electron mass
$\mathfrak{u}$	Nuclear magnetic moment operator
ω	Nuclear excitation energy
Ω	Solid angle
p,p'	Incident and scattered electron momenta, respectively
q	Momentum transfer
R_c	Nuclear charge radius
R_m	Nuclear matter radius
R_{tr}	Nuclear transition radius
s	Nuclear spin
σ	General term for cross section
$\boldsymbol{\sigma}$	Pauli spin operator
τ	Isospin operator (τ_3, its third component)
T	Isospin quantum number
θ	Angle of electron scattering
Z	Nuclear charge

VI. CONCLUSIONS AND SUGGESTIONS FOR FURTHER STUDY

If one considers the early Stanford survey work on electroexcitation of M1 transitions to be the first phase of a progression to more refined measurements, then the second phase made possible by the laboratories at Darmstadt, Amsterdam, NBS, Saclay, Saskatchewan, Glasgow, Maine, and NRL is now drawing to a close. The third phase generated by the development of the energy loss (dispersion matching) technique is already underway with such systems having recently become operational at Darmstadt and MIT.

Clearly much of the work done in the second phase should be repeated. This is certainly true of work in the s–d shell, particularly the upper part of the shell. A careful study of ^{32}S is especially needed. There are also some nuclei in the p-shell that should be re-examined, outstanding candidates being ^{10}B and ^{14}N.

Although the high energy electron scattering studies of nuclei in the s shell command the most current interest, more accurate low-q measurements would still be useful. In this connection the work currently progressing on ^{3}He and ^{3}H at NBS and NRL should be helpful.

The nuclei with $A > 40$ constitute a relatively unexplored region. Closed shell, or near closed, nuclei where spin-flip transitions are more possible have naturally been receiving the most attention. The situation among these nuclei needs much clarification, and the question of the existence of a general giant M1 resonance will probably keep them in high priority for observation for some time.

VII. ACKNOWLEDGMENTS

The author expresses his deep gratitude for the support and invaluable interaction that he has received over the last eight years from his two primary co-workers, Drs. W. Bendel and E. Jones. Other co-workers who have been extremely helpful are Dr. N. Ensslin, Dr. R. Lindgren, Mr. R. Tobin, Miss S. Numrich, Dr. H. Kaiser, Dr. L. Cohen, and Dr. T. Godlove. The critical reading of the manuscript by Drs. G. Peterson, H. Überall, W. Bendel, P. de Witt-Huberts, and T. Godlove is greatly appreciated. The author is very grateful for enlightening discussions with Drs. H. Überall, R. Adler, and M. Rosen. He also wishes to express his gratitude to Ms. B. Sands and Ms. J. Sampson for their excellent typing work, which was only exceeded by their gracious forbearance.

REFERENCES

Adler, R. J., 1966, Phys. Rev. **141**, 1499.
Adler, R. J., 1968, Phys. Rev. **169**, 1192.
Adler, R. J., 1973, private communication.
Adler, R. J., and S. D. Drell, 1964, Phys. Rev. Lett. **13**, 349.
Andresen, H., 1974, private communication.
Artus, H., P. Brix, H. G. Clerc, F. Eigenbrod, A. Goldmann, F. Gudden, E. Spamer, P. Strehl, M. Stroetzel, O. Titze, and K. J. Wetzel, 1967, in *Proceedings of the International Nuclear Physics Conference*, Gatlinburg, Tennessee, edited by R. L. Becker, C. D. Goodman, P. H. Stelson, and A. Zucker (Academic, New York), p. 314.
Baglan, R. J., C. D. Bowman, and B. L. Berman, 1971, Phys. Rev. C **3**, 672.
Barber, W. C., 1962, Annu. Rev. Nucl. Sci. **12**, 1.
Barber, W. C., and F. E. Gudden, 1959, Phys. Rev. Lett. **3**, 219.
Barber, W. C., F. Berthold, G. Fricke, and F. E. Gudden, 1960, Phys. Rev. **120**, 2081.
Barber, W. C., J. Goldemberg, G. A. Peterson, and Y. Torizuka, 1963, Nucl. Phys. **41**, 461.
Barber, W. C., and G. J. Vanpraet, 1965, Nucl. Phys. **72**, 63.
Beer, G. A., P. Brix, H. G. Clerc, and B. Laube, 1968, Phys. Lett. **26B**, 506.
Belyi, Yu. I., and N. M. Kabachnik, 1972, Sov. J. Nucl. Phys. **14**, 619.
Bendel, W. L., 1972, private communication.
Bendel, W. L., L. W. Fagg, R. A. Tobin, and H. F. Kaiser, 1968, Phys. Rev. **173**, 1103.
Bendel, W. L., L. W. Fagg, S. K. Numrich, E. C. Jones, Jr., and H. F. Kaiser, 1971, Phys. Rev. C **3**, 1821.
Bendel, W. L., E. C. Jones, L. W. Fagg, R. A. Lindgren, and F. E. Cecil, 1973, to be published.
Bendel, W. L., E. C. Jones, and L. W. Fagg, 1974, Bull. Am. Phys. Soc., Ser. II **19**, 999.
Bergstrom, J. C., 1967, M.I.T. Laboratory for Nuclear Science Report LNS116 (May 1967), unpublished; and *Proceedings of M.I.T. Summer Study* TID 24667, p. 207.
Bergstrom J. C., I. P. Auer, M. Ahmad, F. J. Kline, J. H. Hough, H. S. Caplan, and J. L. Groh, 1973, Phys. Rev. C **7**, 2228.
Bernheim, M., 1965, Thesis, University of Paris, Orsay, unpublished.
Bernheim, M., and G. R. Bishop, 1963, Phys. Lett. **5**, 294.
Bernheim, M., and G. R. Bishop, 1963a, J. Phys. Radium **24**, 970.
Bishop, G. R., 1973, J. Phys. A **6**, L21.
Bishop, G. R., and M. Bernheim, 1963, Phys. Lett. **5**, 140.
Bishop, G. R., M. Bernheim, and P. Kossanyi-Demay, 1964, Nucl. Phys. **54**, 353.
Blankenbecler, R., and J. F. Gunion, 1971, Phys. Rev. D **4**, 718.
Blatt, J. M., and V. F. Weisskopf, 1952, *Theoretical Nuclear Physics* (Wiley, New York).
Borie, E., 1970, Phys. Rev. C **2**, 770.
Bosco, B., P. P. Delsanto, and F. E. Erdas, 1964, Nuovo Cimento **33**, 1240.
Bowman, C. D., R. J. Baglan, B. L. Berman, and T. W. Philips, 1970, Phys. Rev. Lett. **25**, 1302.
Cardman, L. C., S. P. Fivozinsky, J. S. O'Connell, and S. Penner, 1973, Bull. Am. Phys. Soc. **18**, 78.
Castel, B., I. P. Johnstone, B. P. Singh, and J. C. Parikh, 1970, Nucl. Phys. A **157**, 137.
Cecil, F. E., W. L. Bendel, E. C. Jones, and L. W. Fagg, 1973, to be published.
Cecil, F. E., L. W. Fagg, W. L. Bendel, and E. C. Jones, 1974, Phys. Rev. C **9**, 798.
Chertok, B. T., 1969, Phys. Rev. **187**, 1340.
Chertok, B. T., and E. C. Booth, 1965, Nucl. Phys. **66**, 230.
Chertok, B. T., and W. T. K. Johnson, 1969, Phys. Rev. Lett. **22**, 67.
Chertok, B. T., E. C. Jones, W. L. Bendel, and L. W. Fagg, 1969, Phys. Rev. Lett. **23**, 34.
Chertok, B. T., W. T. K. Johnson, and D. Sarkar, 1970, Phys. Rev. C **2**, 2028.
Chertok, B. T., W. T. K. Johnson, and D. Sarkar, 1970a, *Table of Coulomb Distortion Corrections to Inelastic Electron Scattering Cross Sections for Magnetic Dipole and Quadrupole Transitions* (American University, Washington, D. C.).
Chertok, B. T., C. Sheffield, J. W. Lightbody, Jr., S. Penner, and D. Blum, 1973, Phys. Rev. C **8**, 23.
Clerc, H. G., 1968, Habilitationsschrift, Technische Hochschule Darmstadt.
Clerc, H. G., K. J. Wetzel, and E. Spamer, 1966, Phys. Lett. **20**, 667.
Clerc, H. G., and E. Kuphal, 1968, Z. Phys. **211**, 452.
Clerc, H. G., K. J. Wetzel, and E. Spamer, 1968, Nucl. Phys. A **120**, 441.
Crannell, H., 1969, Nucl. Instrum. Methods **71**, 208.
Crannell, H., P. L. Hollowell, J. N. Finn, J. T. O'Brien, N. Ensslin, L. Fagg, W. Bendel, and E. Jones, 1973, Bull. Am. Phys. Soc. **18**, 669.
Davis, R., L. C. Rogers, and V. Aadenka, 1971, Bull. Am. Phys. Soc. **16**, 631.
deVries, C., 1963, Stanford Linear Accelerator Report SLAC-25, p. 160, unpublished.
deVries, C., 1972, in *Nuclear Structure Studies using Electron Scattering and Photoreaction*, edited by K. Shoda and H. Ui (Tohoku University, Sendai, Japan), p. 405.
Dieperink, A. E. L., 1973, private communication.
Donnelly, T. W., J. D. Walecka, I. Sick, and E. G. Hughes. 1968, Phys. Rev. Lett. **21**, 1196.
Drechsel, D., 1967, *Medium Energy Nuclear Physics with Electron Linear Accelerators*, M.I.T. Summer Study, M.I.T.-2098-#470, p. 186.
Drechsel, D., 1968, Nucl. Phys. A **113**, 665.
Drake, T., E. L. Tomusiak, and H. S. Caplan, 1968, Nucl. Phys. A **118**, 138.
Drake, T. E., and R. P. Singhal, 1972, Internal Report, Kelvin Laboratory, University of Glasgow, Scotland.
Dudelzak, B., and R. E. Taylor, 1961, J. Phys. Radium **22**, 544.
Durand, L., 1961, Phys. Rev. **123**, 1393.
Edge, R. D., and G. A. Peterson, 1962, Phys. Rev. **128**, 2750.
Eigenbrod, F., 1969, Z. Phys. **228**, 337.
Endt, P. M., and C. Van der Leun, 1967, Nucl. Phys. A **105**, 1.
Ensslin, N., 1973, private communication.
Ensslin, N., W. L. Bendel, L. W. Fagg, T. F. Godlove, and E. C. Jones, 1973, Bull. Am. Phys. Soc. Ser. II **18**, 670.
Ensslin, N., W. Bertozzi, S. Kowalski, C. P. Sargent, S. P. Fivozinsky, J. W. Lightbody, Jr., and S. Penner, 1974, Phys. Rev. C **9**, 1705.
Fagg, L. W., 1973, in *Proceedings of the International Conference on Photonuclear Reactions and Applications*, Asilomar Conference

Grounds, Pacific Grove, California, edited by B. L. Berman (Lawrence Livermore Laboratory, Livermore), Vol. 1, 663.
Fagg, L. W., and S. S. Hanna, 1959, Rev. Mod. Phys. **31**, 711.
Fagg, L. W., W. L. Bendel, R. A. Tobin, and H. F. Kaiser, 1968, Phys. Rev. **171**, 1250.
Fagg, L. W., W. L. Bendel, E. C. Jones, Jr., and S. Numrich, 1969, Phys. Rev. **187**, 1378.
Fagg, L. W., W. L. Bendel, E. C. Jones, Jr., H. F. Kaiser, and T. F. Godlove, 1969a, Phys. Rev. **187**, 1384.
Fagg, L. W., E. C. Jones, and W. L. Bendel, 1970, Nucl. Instrum. Methods **77**, 136.
Fagg, L. W., W. L. Bendel, S. K. Numrich, and B. T. Chertok, 1970a, Phys. Rev. C **1**, 1137.
Fagg, L. W., W. L. Bendel, L. Cohen, E. C. Jones, Jr., H. F. Kaiser, and H. Uberall, 1971, Phys. Rev. C **4**, 2089.
Fagg, L. W., W. L. Bendel, E. C. Jones, Jr., L. Cohen, and H. F. Kaiser, 1972, Phys. Rev. C **5**, 120.
Fagg, L. W., W. L. Bendel, N. Ensslin, and E. C. Jones, 1973, Phys. Lett. **44B**, 163.
Fagg, L. W., W. L. Bendel, E. C. Jones, N. Ensslin, and F. E. Cecil, 1973a, in *Proceedings of the International Conference on Nuclear Physics*, Munich, edited by J. de Boer and H. J. Mang (North-Holland, Amsterdam), Vol. 1, p. 631.
Fetisov, V. M., and Yu. S. Kopysov, 1972, Phys. Lett. **40B**, 602.
Flynn, E. R., and J. D. Garrett, 1972, Phys. Rev. Lett. **29**, 1748.
Flynn, E. R., J. Sherman, and N. Stein, 1974, Phys. Rev. Lett. **32**, 846.
Fowler, W. A., 1972, Nature **238**, 24.
French, J. B., and M. H. MacFarlane, 1961, Nucl. Phys. **26**, 168.
Ganichot, D., D. Benaksas, B. Grossetete, J. Lorrain, and D. B. Isabelle, 1968, Nucl. Instrum. Methods **60**, 151.
Ganichot, D., B. Grossetete, and D. B. Isabelle, 1972, Nucl. Phys. A **178**, 545.
Gargaro, W. W., and D. S. Onley, 1971, Phys. Rev. C **4**, 1032.
Ginsberg, E. S., and R. H. Pratt, 1964, Phys. Rev. B **134**, 773.
Goldemberg, J., W. C. Barber, F. H. Lewis, Jr., and J. D. Walecka, 1964, Phys. Rev. B **134**, 1022.
Goldemberg, J., and R. H. Pratt, 1966, Rev. Mod. Phys. **38**, 311.
Goldemberg, J., and C. Schaerf, 1966, Phys. Lett. **20**, 193.
Goldmann, A., and M. Stroetzel, 1970, Phys. Lett. B **31**, 287.
Gudden, F., 1964, Phys. Lett. **10**, 313.
Gudden, F., G. Fricke, H. G. Clerc, and P. Brix, 1964, Z. Phys. **181**, 453.
Gulkarov, I. S., N. G. Afanasyev, G. A. Savitsky, V. M. Khvastunov, and N. G. Shevchenko, 1968, Phys. Lett. **27B**, 417.
Hadjimichael, E., 1973, Phys. Lett. **46B**, 147.
Hanna, S. S., 1969, in *Isospin in Nuclear Physics*, edited by D. H. Wilkinson (North-Holland, Amsterdam), p. 593.
Hanna, S. S., 1974, invited paper at International Conference on Nuclear Structure and Spectroscopy, Amsterdam.
Harvey, J. A., W. M. Good, N. W. Hill, and R. H. Schindler, 1973, Contribution to 1973 Physics Division Annual Report, Argonne National Laboratory, Argonne, Ill.
Hutcheon, R. M., T. E. Drake, V. W. Stobie, G. A. Beer, and H. S. Caplan, 1968, Nucl. Phys. A **107**, 266.
Hutcheon, R. M., and H. S. Caplan, 1969, Nucl. Phys. A **127**, 417.
Hutcheon, R. M., R. Neuhausen, and F. Eigenbrod, 1970, Z. Naturforsch. **25a**, 973.
Isabelle, D. B., and J. Berthot, 1960, "Radiative Corrections from an Experimentalist's View Point," presented at Institute on Electron Scattering and Nuclear Structure, Cagliari, Italy.
James, A. N., P. R. Alderson, D. C. Bailey, P. E. Carr, J. L. Burell, M. A. Greene, and J. F. Sharpey-Schafer, 1971, Nucl. Phys. A **172**, 401.
Jankus, V. Z., 1956, Phys. Rev. **102**, 1586.
Johnston, A., and T. E. Drake, 1974, J. Phys. **7**, 898.
Jones, E. C., 1974, private communication.
Jones, E. C., and B. T. Chertok, 1968, unpublished.
Kan, P. T., G. A. Peterson, D. V. Webb, S. P. Fivozinsky, J. W. Lightbody, and S. Penner, 1974, Phys. Rev. C **11**, 323.
Koerts, L. A. C., 1964, Nucl. Instrum. Methods **26**, 152.
Kossanyi-Demay, P., and G. J. Vanpraet, 1966, Nucl. Phys. **81**, 529.
Kossanyi-Demay, P., and G. J. Vanpraet, 1966a, Stanford University preprint HEPL 394.
Kowalski, S., and H. Enge, 1972, in *Proceedings of the Fourth International Conference on Magnet Technology*, Upton, N. Y., edited by Y. Winterbottom (National Technical Information Service, Springfield, Va.), 182.
Kuehne, H. W., P. Axel, and D. C. Sutton, 1967, Phys. Rev. **163**, 1278.
Kurath, D., 1956, Phys. Rev. **101**, 216.
Kurath, D., 1963, Phys. Rev. **130**, 1525.
Kurath, D., 1964, Phys. Rev. **134**, B1025.
Kurath, D., 1972, Phys. Rev. C **5**, 768.
Lapikas, L., 1970, Master's Thesis, Institut voor Kernphysisch Onderzoek, Amsterdam.
Lapikas, L., A. E. L. Dieperink, and G. Box, 1973, Nucl. Phys. A **203**, 609.
Lapikas, L., H. deVries, and G. Box, to be published.
Leconte, P., 1967, in *Proceedings of M.I.T. Summer Study* TID 24667, pp. 199–200.
Lee, H. C., 1974, private communication.
Lees, E. W., A. Johnston, S. W. Brain, C. S. Curran, W. A. Gillespie, and R. P. Singhal, 1974, J. Phys. A **7**, 936.
Liesem, H., 1966, Z. Phys. **196**, 174.
Lindgren, R. A., 1974, private communication.
Lindgren, R. A., W. L. Bendel, E. C. Jones, L. W. Fagg, X. K. Maruyama, J. W. Lightbody, and S. P. Fivozinsky, 1974, to be published.
Lombard, R. M., and G. R. Bishop, 1967, Nucl. Phys. A **101**, 601.
Lombard, R. M., and G. R. Bishop, 1967a, Nucl. Phys. A **101**, 625.
Lone, M. A., L. W. Fagg, W. L. Bendel, E. C. Jones, Jr., X. K. Maruyama, and R. A. Lindgren, 1974, Bull. Am. Phys. Soc. **19**, 111.
Lone, M. A., W. L. Bendel, R. A. Lindgren, E. C. Jones, L. W. Fagg, and F. E. Cecil, 1974a, to be published.
Maripuu, S., and B. H. Wildenthal, 1972, Phys. Lett. **38B**, 464.
Maruyama, X. K., R. A. Lindgren, W. L. Bendel, E. C. Jones, Jr., and L. W. Fagg, 1974, Phys. Rev. C **10**, 2257.
Maximon, L. C., 1969, Rev. Mod. Phys. **41**, 193.
Maximon, L. C., 1970, unpublished notes.
Maximon, L. C., and D. B. Isabelle, 1964, Phys. Rev. **136**, B674.
McCormick, P. T., D. G. Keiffer, and G. Parzen, 1956, Phys. Rev. **103**, 29.
Metzger, F. R., 1971, Ann. Phys. (N. Y.) **66**, 697.
Mo, L. W., and Y. S. Tsai, 1969, Rev. Mod. Phys. **41**, 205.
Morpurgo, G., 1958, Phys. Rev. **110**, 721.
Motz, J. W., H. Olsen, and H. W. Koch, 1964, Rev. Mod. Phys. **36**, 881.
Neuhausen, R., and R. M. Hutcheon, 1971, Nucl. Phys. A **164**, 497.
Nilsson, S. G., 1955, K. Dan. Vidensk. Selsk. Mat.-Fys. Medd. **29**, 1.
O'Brien, J. T., H. Crannell, and F. J. Kline, 1974, Phys. Rev. C **9**, 1418.
O'Connell, J. S., T. W. Donnelly, and J. D. Walecka, 1972, Phys. Rev. C **6**, 716.
O'Connell, J. S., and B. F. Gibson, 1973, private communication.
Penner, S., 1973 private communication.
Peterson, G. A., 1962, Phys. Lett. **2**, 162.
Peterson, G. A., 1967, Phys. Lett. **25B**, 549.
Peterson, G. A., 1968, Nucl. Instrum. Methods **59**, 341.
Peterson, G. A., 1973, private communication.
Peterson, G. A., and W. C. Barber, 1962, Phys. Rev. **128**, 812.
Peterson, G. A., and D. Vetter, 1974, private communication.
Pham, T. N., 1972, Nucl. Phys. A **185**, 413.
Pham, T. N., 1972a, Phys. Rev. Lett. **29**, 1111.
Pham, T. N., 1973, to be published.
Pitthan, R., 1973, Z. Phys. **260**, 283.
Pitthan, R., and T. Walcher, 1971, Phys. Lett. **36B**, 563.
Pitthan, R., and T. Walcher, 1972, Z. Naturforsch. **27a**, 1683.
Preedom, B. M., and B. H. Wildenthal, 1972, Phys. Rev. C **6**, 1633.
Proca, G., 1966, Thesis L.A.L. 1150 (Orsay, 1966), unpublished.
Proca, G. A., and D. B. Isabelle, 1968, Nucl. Phys. A **109**, 177.
Rand, R. E., 1966, Nucl. Instrum. Methods **39**, 45.
Rand, R. E., 1972, Rev. Sci. Instrum. **43**, 352.
Rand, R. E., R. Frosch, and M. R. Yearian, 1966, Phys. Rev. **144**, 859.
Ring, P., and J. Speth, 1974, Nucl. Phys. A **235**, 315.
Rose, H. J., O. Hausser, and E. K. Warburton, 1968, Rev. Mod. Phys. **40**, 591.
Rosen, M., 1973, private communication.
Rosen, M., R. Raphael, and H. Überall, 1967, Phys. Rev. **163**, 927.
Siegert, A. J. F., 1937, Phys. Rev. **52**, 787.
Slight, A. G., T. E. Drake, and G. R. Bishop, 1973, Nucl. Phys. A **208**, 157.
Smirnov, S. A., and S. V. Trubnikov, 1974, Phys. Lett. **48B**, 105.
Spamer, E., 1966, Z. Phys. **191**, 24.
Spamer, E., 1973, private communication.
Spamer, E., and F. Gudden, 1965, Phys. Lett. **14**, 210.
Spamer, E., and H. Artus, 1967, Z. Phys. **198**, 445.
Spamer, E., K. Gravemeyer, C. W. deJager, and L. Dieperink, 1972, in *Nuclear Structure Studies Using Electron Scattering and Photoreaction*, edited by K. Shoda and H. Ui (Tohoku University, Sendai, Japan), p. 419.
Stroetzel, M., and A. Goldmann, 1970, Z. Phys. **233**, 245.

Swann, C. P., 1974, Phys. Rev. Lett. **32**, 1449.
Theissen, H., 1972, Springer Tracts Mod. Phys. **65**, 1.
Theissen, H., R. J. Peterson, W. J. Allston, and J. R. Stewart, 1969, Phys. Rev. **186**, 1119.
Titze, O., 1969, Z. Physik **220**, 66.
Titze, O., and E. Spamer, 1966, Z. Naturforsch **21a**, 1504.
Titze, O., E. Spamer, and A. Goldmann, 1967, Phys. Lett. **24B**, 169.
Toohey, R. E., and H. E. Jackson, 1972, Phys. Rev. C **6**, 1440.
Trimble, V., and F. Reines, 1973, Rev. Mod. Phys. **45**, 1.
Tuan, S. T., L. W. Wright, and D. S. Onley, 1968, Nucl. Instrum. Methods **60**, 70.
Twin, P. J., W. C. Olsen, and D. M. Sheppard, 1970, Nucl. Phys. A **143**, 481.
Überall, H., 1971, *Electron Scattering from Complex Nuclei* (Academic, New York).
Überall, H., 1973, private communication.
Vanpraet, G. J., and P. Kossanyi-Demay, 1969, Z. Phys. **222**, 455.
VanNiftrik, G. J. C., H. deVries, L. Lapikas, and C. deVries, 1971, Nucl. Instrum. Methods **93**, 301.
VanNiftrik, G. J. C., L. Lapikas, H. deVries, and G. Box, 1971a, Nucl. Phys. A **174**, 173.
Vergados, J. D., 1971, Phys. Lett. **36B**, 12.
Walcher, T., 1973, private communication.
Webb, D. V., G. A. Peterson, L. W. Fagg, W. L. Bendel, and E. C. Jones, 1974, to be published.
Wechsung, R., W. Strassheim, and R. Bass, 1971, Nucl. Phys. A **170**, 557.
Wildenthal, B. H., 1973, private communication.
Wittwer, G., H. G. Clerc, and G. A. Beer, 1970, Z. Phys. **234**, 120.
Wolf, A., R. Moreh, A. Nif, O. Shahal, and J. Tenebaum, 1972, Phys. Rev. C **6**, 2276.
Yoshida, S., and L. Zamick, 1972, Annu. Rev. Nucl. Sci. **22**, 121.